Toward Bi^{3+} red luminescence with no visible reabsorption through manageable energy interaction and crystal defect modulation in single Bi^{3+}-Doped $ZnWO_4$ crystal

Jin Han,[1] Fengwen Kang,[*2] Mingying Peng,[*1] Bolong Huang,[*2] Fengjuan Pan,[3] Liyi Li,[1] Lejing Li,[1] Jing Wang,[4] and Bingfu Lei,[5]

[1] The China-Germany Research Center for Photonic Materials and Devices, The State Key Laboratory of Luminescent Materials and Devices, and Guangdong Provincial Key Laboratory of Fiber Laser Materials and Applied Techniques, School of Materials Science and Engineering, South China University of Technology, Guangzhou 510641; [2] Department of Applied Physics, and Department of Applied Biology and Chemical Technology, The Hong Kong Polytechnic University, Hung Hom, Kowloon, Hong Kong SAR, China; [3]College of Chemistry and Molecular Engineering, Peking University, Beijing 100871,China; [4] School of Chemistry, Sun Yat-Sen University, Guangzhou 510275; [5] The College of Materials and Energy, South China Agricultural University, Guangzhou 510640;.

ABSTRACT

The last decades have witnessed the discovery of tens of thousands of rare earth (RE) (*e.g.*, Eu^{2+}, Tb^{3+}) and non-RE (*e.g.*, Mn^{2+}, Cr^{3+}) related photonic materials for near ultraviolet (NUV) and blue converted white light-emitting diodes (wLEDs), but the future development of wLEDs technology are constrained greatly by the intrinsic problems of these dopants, such as, the visible light reabsorption, the unchanged emission lines and the limited absorption ability in UV/blue region. Here we report a new strategy to discover novel Bi^{3+} red luminescent materials by the guidance of the density functional theory (DFT) calculation, which can smoothly address the above problems eventually. Specifically, we first discuss the unique structural feature of bulk $ZnWO_4$ crystal, followed by screening all possible types of Bi doping through the projected partial density of states (PDOSs). Our DFT findings reveal that doping Bi enables bulk $ZnWO_4$ to be of potential in modulating the output luminescence. As confirmed by experiment, manipulating the monitored energy enables tuning the emission peaks from 490 nm to 680 nm and simultaneously controlling the distribution of the Bi^{3+} excitation intensity over the whole near-UV spectral region. In addition, as temperature is increased to 300 K from 10 K, the emission positions upon excitation at 360 nm feature a redshifting from 626 nm to 688 nm followed by a subsequent blueshifting to 654 nm; while exciting at 270 nm only gives rise to blueshifting the peak from 500 nm to 484 nm. Analysis on DFT and spectral results reveals that the manageable energy transfer between $ZnWO_4$ host and Bi^{3+}, the V_{ZnO} defect perturbation in the $ZnWO_4$ and the $2Bi_{Zn}V_W$ complex which is produced by substitution of Zn site with Bi^{3+} are the reasons for the tunable emissions, and they lead to the anomalous Bi^{3+} red luminescence eventually. This work not only provides a new insight into exploring more compounds which could allow Bi emitting red light only upon the excitation of near-UV light, but also improves our understanding on the complicated energy interactions between Bi dopant and host lattice, which, therefore, represents a new directive strategy for researchers to study the undiscovered luminescence properties in Bi^{3+} or other ions (*e.g.*, Eu^{2+}, and Mn^{2+}) doped systems.

***Corresponding Authors**

[1] *Prof.* Mingying Peng, South China University of Technology, Guangzhou 510641, China; **Email address*: pengmingying@scut.edu.cn.

[2] *Dr.* Fengwen Kang, and *Dr.* Bolong Huang, The Hong Kong Polytechnic University, Kowloon, Hong Kong SAR; **Email address*: fenwen.kang@polyu.edu.hk, and bhuang@polyu.edu.hk.

1. INTRODUCTION

Ever since the first-time success in implementing phosphor-converted white light-emitting diodes (pc-wLEDs) through depositing a layer of yellow-emitting YAG:Ce^{3+} phosphor on an InGaN blue-emitting LEDs chip by Nakamura and his coworkers in 1997,[1] pc-wLEDs technology has been rapidly accepted as one of the best strategies to pump warm white light. The pc-wLEDs technology possesses a wealth of advantages compared to conventional lighting technologies (*e.g.*, fluorescent and incandescent lamps), including smaller and compacter size, higher output luminous efficiency, faster switching, less energy consumption, and lower working temperature.[2-4] As a result, people can benefit a lot from this technology in a wide range of fields, *e.g.*, general indoor and outdoor lighting, screen backlight source, traffic signal, liquid crystal display (LCD), computer tough panels, architectural decoration, agricultural technology, automobiles, *etc*.[5-8] Currently, it can be said without any exaggeration that the technology is changing and will continue to change our daily life. As indicated by the design concept, however, most popular pc-wLEDs cannot work well without involving phosphors. Because of this, extensive efforts have been devoted over the past decades in order to find new phosphors that can match well with commercial LED chip, typically near-UV and blue chip. According to a conservative estimation through *ISI* web of science, tens of thousands of phosphors, thus, have been developed.

For phosphors that can work together with near-UV and blue chip, they basically can be categorized as two basic classes: RE (*e.g.*, Eu^{2+}, Ce^{3+}, Dy^{3+}, Tb^{3+}, Eu^{3+}, Sm^{3+}, Pr^{3+}, *etc*) and non-RE related (*e.g.*, Mn^{2+}, Mn^{4+}, Cr^{3+}, *etc*) photonic materials. Until now, various visible colors based on these dopants have become available, *i.e.*, (i) green light, $NaCaPO_4:Tb^{3+}$ (~547 nm),[9] $Ca_3Sc_2Si_3O_{12}:Ce^{3+}$ (~505 nm),[10] $Ba_2LiSi_7AlN_{12}:Eu^{2+}$ (~515 nm);[11] (ii) blue light, $Ba_2Y_5B_5O_{17}:Ce^{3+}$ (~443 nm);[12] (iii) red light, $Y_2O_2S:Eu^{3+}$ (~616 nm),[13] $Sr[LiAl_3N_4]:Eu^{2+}$ (650 nm),[14] $NaGdTiO_4:Pr^{3+}$ (~624 nm)[15], $Sr_2CaMoO_6:Sm^{3+}$ (~650 nm),[16] $CaMg_2Al_{16}O_{27}:Mn^{4+}$ (~655 nm),[17] $Ca_{2.5}Sr_{0.5}Al_2O_6:Mn^{2+}$ (~610 nm);[18] (iv) yellow light, $Ca_{1.5}Ba_{0.5}Si_5O_3N_6:Eu^{2+}$ (~590 nm),[19] $Y_3Al_5O_{12}:Ce^{3+}$ (~565 nm),[8] $Sr_3In(PO_4)_3:Mn^{2+}$ (~573 nm);[20] (v) complex light due to multi emission components, $Ba_{1.55}Ca_{0.45}SiO_4:Mn^{2+}$ (595 nm, red-orange),[21] $YVO_4:Dy^{3+}$ (483 nm and 574 nm, blue-yellow),[22] *etc*. Additionally, confining multi-activators into a single crystal host sometimes also enables achieving tunable colors over the visible spectral region, for instance, (Gd-Y-Bi-Eu)VO_4 (green → red),[23] $BaMg_2Al_6Si_9O_{30}:Eu^{2+}$, Tb^{3+}, Mn^{2+} (full visible color),[24] $NaGd(WO_4)_2:Tm^{3+}$, Dy^{3+}, Eu^{3+} (purple → blue → white → red),[25] $Ba_{1.55}Ca_{0.45}SiO_4:Eu^{2+}$, Mn^{2+} (blue → yellow),[21] $KNaCa_2(PO_4)_2$:A (A=Ce^{3+}, Eu^{2+}, Tb^{3+}, Mn^{2+}, Sm^{3+}) (blue → white → reddish/orange).[26] Obviously, the reason why these activators can emit so many colors is because they feature the unique electron configurations of the well-shielded 4f electrons (*i.e.*, Tb^{3+}, Eu^{3+} and Pr^{3+}), the *d-f* transition (*i.e.*,

Eu^{2+}, Dy^{3+}, and Ce^{3+}), the $^4T_1(^4G)\rightarrow{}^6A_1(^6S)$ transition (*i.e.*, Mn^{2+}), the $^2E_g\rightarrow{}^4A_2$ transition (*i.e.*, Mn^{4+}), and the $^2E\rightarrow{}^4A_2$ transition (*i.e.*, Cr^{3+}). However, it is also because of such electron configurations, doping of phosphors with these activators frequently induces severe problems such as the broad excitation bands in the visible spectral region (*e.g.*, Eu^{2+}, Ce^{3+}, Dy^{3+}, Mn^{2+}, Mn^{4+}, Cr^{3+}, *etc*), the single emission color resulting from the unchanged lines (*e.g.*, Tb^{3+}, Eu^{3+}, Pr^{3+}, *etc*), the insensitive emission color for human eyes (*e.g.*, Mn^{4+}, Cr^{3+}, *etc*), the limited absorption ability in UV/blue region (<10 nm) and the UV leakage for human health (*e.g.*, Tb^{3+}, Eu^{3+}, Sm^{3+}, Pr^{3+}, *etc*). As a result of these problems, the application and the future development of pc-WLEDs technology are challenged greatly. Moreover, when compared with other phosphors, typically the blue and green phosphors, red phosphors show relatively lower luminescence efficiency, leading to consume more red phosphors in the pc-WLEDs fabrication process. Thus, developing lower cost red phosphor that can prevent the visible light reabsorption is extremently important for pc-WLEDs.

Trivalent bismuth (Bi^{3+}) has been known to possess the unique [Xe] $4f^{14}5d^{10}6s^2$ electronic configuration, and therefore it is very sensitive to the crystal-field and the environment of crystal host lattice. As a result of this behavior, Bi^{3+} enables emitting various colors, spanning from UV to yellow and even red in $ScVO_4:Bi^{3+}$.[27] Based on the well-reported Bi^{3+} phosphors, strong absorption in UV but not in visible region seems the unique excitation spectral feature for single Bi^{3+} doped phosphors. This can be vividly shown by the following example, *i.e.*, manipulating the cation ratios of $(Y, Lu, Sc)VO_4:Bi$[28] and $(Y, Sc)(Nb, V)O_4:Bi$[29] phosphors enable tuning the excitation range, but the tail terminates only at ~420 nm. More remarkably, when compared Bi^{3+} with Mn^{2+}, Eu^{2+} and Ce^{3+}, we can find that they share many similar spectral features, including broad excitation and emission bands, sensitive to coordination-environment and crystal-field. Moreover, these dopants also show the tunable emissions, *e.g.*, $KMg_{(1-x)}F_3:Mn_x^{2+}$ (x=0.01 → 1.0, λ_{em}=600 nm → 780 nm),[30] $(K_{1-x}, Na_x)SrPO_4:Eu^{2+}$ (x=0 → 0.6, λ_{em}=446 nm → 498 nm),[31] $Y_4Si_2O_7N_2:xCe^{3+}$ (x=0.1 mol% → 10 mol%, λ_{em}=450 nm → 515 nm),[32] $(Y, Lu)VO_4:Bi^{3+}$ (Y → Lu, λ_{em}=566 nm → 576 nm).[28] For the red spectral aspect, however, they show a completely different situation. In Mn^{2+}, Eu^{2+} and Ce^{3+} doped aluminates,[18] silicates,[33] sulfides,[34] nitrides,[14] and nitrogen oxides phosphors[35], red emissions are reported frequently. For Bi^{3+} phosphors, however, except for $ScVO_4:Bi^{3+}$ red phosphor,[36] previous reports focus mainly on the light from UV to yellow. The red light from Bi^{3+} seems to have been solely hidden and, thus, this looks extremely strange and also confuses us for a long time. Fortunately, because of the discovery of $ScVO_4:Bi^{3+}$ red phosphor, there should be some undiscovered Bi^{3+} red emission in other materials. Then the periodic table indicates us that, unfortunately, there are so many elements and, based on them, a large number of crystal candidates

suitable for Bi^{3+} doping can be achieved. This indicates us that how to seek suitable crystal lattice that can allow Bi^{3+} emitting required luminescence typically red emission is a challenging yet important subject.

As one fascinating member of inorganic materials, the wolframite-type zinc tungstate ($ZnWO_4$) crystallizes in the monoclinic structure with the space group of *P*12/*c*1 (No.13).[37] Based on the $ZnWO_4$ crystal structure (**Figure 1**(**a**)), both Zn site (2*f*) and the W site (2*e*) are coordinated by six oxygen atoms, leading to the formation of ZnO_6 and WO_6 octahedra structure. Two interconnected zigzag chains, which consist of ZnO_6 and WO_6 octahedra, extend individually along the *c*-axis. Since the six-oxygen coordinated Zn^{2+} and W^{6+} radii are 0.74 Å and 0.60 Å, respectively, it normally consider that the Zn^{2+} or W^{6+} sites are impossible to be replaced by the bigger Bi^{3+} ion (where the Bi^{3+} radius for six-oxygen coordination is 1.03 Å). In consequence, studies on the photoluminescence property of Bi^{3+} doped $ZnWO_4$ crystal are seldom noticed by previous works, although various applications based on $ZnWO_4$ crystal, such as photocatalytic degradation, Li-ion batteries, laser techniques, supercapacitor, hybridized semiconductor, electronic and optoelectronic systems, and scintillator,[37-39] are reported frequently. A closer re-inspection into the $ZnWO_4$ crystal reveals that only one type of Zn^{2+}, W^{6+} and O^{2-} situates in $ZnWO_4$ crystal, and the ZnO_6 chains are corner-linked to four WO_6 chains by sharing oxygen atoms, resulting in a tightly manageable interaction between the ZnO_6 and WO_6 octahedra. From the projected density of states (PDOS) of $ZnWO_4$ crystal through the DFT calculations (**Figure 1**(**b**)), the optical band gap (E_g) of bulk $ZnWO_4$, which defines as the difference between the valence band maximum (VBM) and the conduction band minimum (CBM), is ~4.019 eV. The O-2p and the W-5d orbital levels have dominantly contributed to VB and CB, and their energy band widths are about 6.5 eV and 2.0 eV, respectively. Additionally, the position of Zn-3d orbital levels, which starts from about 7.5 eV below the top of VB, is deeply below the VB, and its energy band width is about 1.0 eV. From the width of these orbital levels, Zn-3d shows smaller than O-2p and W-5d, and the position of the orbital levels between O-2p, W-5d and Zn-3d is different from each other. On basis of these differences, the electronic properties of $ZnWO_4$ crystal would change significantly if Bi^{3+} could successfully build into the $ZnWO_4$ crystal. This change, together the possible tight interaction modulation between the ZnO_6 and WO_6 octahedra, may further allow Bi^{3+} emitting anomalous Bi^{3+} luminescence that differs in the frequently-observed Bi^{3+} luminescence.

In our design, we chose the wolframite-type $ZnWO_4$ as the host material for Bi^{3+} dopant. Followed by screening the projected partial density of states (PDOS) for all possible types of Bi doping in $ZnWO_4$ crystal, we theoretically deduce that doping Bi^{3+} tends to substitute the Zn^{2+} site

to generate the Bi_{Zn} doping type, followed by the generation of the charge compensated complex $2Bi_{Zn}V_W$ and crystal defect V_{ZnO}. This, as confirmed by our experiment, allows us achieving tunable Bi^{3+} luminescence from blue to red light and controllable excitation intensity over the whole near-UV region. Spectral information indicates that the $ZnWO_4:Bi^{3+}$ phosphor is a novel UV converted red phosphor that can be only excited by near-UV light and it therefore shows the potential ability in addressing all intrinsic problems inheriting from Eu^{2+}, Ce^{3+}, Tb^{3+}, Eu^{3+}, Pr^{3+}, Sm^{3+}, Mn^{2+}, Mn^{4+} and Cr^{3+} phosphors. In view of the limited predictive power, we expect this work can provide new directive clues for researchers to discover more crystal hosts that can allow Bi emitting red light and simultaneously find some undiscovered luminescence properties in other RE and non-RE doped phosphor systems, guided by the DFT calculation.

2. COMPUTATIONAL DETAILS

In our work, the geometry relaxation of the lattice was performed at PBE+U in DFT through CASTEP codes,[40] which has been proved that is reliable on many d/f-orbital based oxides.[41] To improve the accuracy of the results of electronic properties, we introduce the recently developed method on ab-initio determination of Hubbard U parameters to carefully avoid extra spurious error from orbital self-interactions.[42-45] We choose different orbitals projectors for different atoms to represent their valence states. For instance, Zn with (3d, 4s, 4p), W with (5s, 5p, 5d, 6s) states and O with (2s, 2p) states have been chosen for pseudopotential generation, respectively. The DFT+U method that developed by Anisimov-type rotational invariant scheme.[46] Regarding the electronic minimization process, the ensemble DFT (EDFT) method of Marzari et al is used for solving Kohn-Sham equation,[47] in order to prevent the charge-spin out-sync sloshing effect and guarantee the electronic minimization and convergence. With a combined convergence test, we select the Baldereschi special k-point (¼, ¼, ¼) in the simple cubic 2×2×2 supercell for fast convergence in energy, to converges the total energy below the tolerance of $5.0x10^{-7}$eV per atom.[48]

3. EXPERIMENTAL DETAILS

3.1 Synthesis of $ZnWO_4:Bi^{3+}$ phosphors

The conventional high temperature solid-state reaction method was employed to synthesize the targeted $ZnWO_4:Bi^{3+}$ phosphors. The experimental reagents involved in this work were ZnO (A. R., "A. R." denotes analytical reagent), WO_3 (A. R.) and Bi_2O_3 (99.999%), and they were used as purchased without further purification. Since we could not confirm the Zn^{2+} and W^{6+} sites in $ZnWO_4$ crystal could be substituted readily by Bi^{3+} ions, we, thus, designed the targeted phosphors with the nominal chemical compositions of $ZnWO_4:xBi^{3+}$ (x = 0.5%, 1.0%, 1.5%, 2.0%, 2.5%, and 3.0%), without considering the occupancy preference of Zn and W sites by Bi^{3+} dopant. With the chemical

stoichiometric molar ratio, we weighed chemical reagents and then mixed them evenly in an agate mortar. After sintering the mixtures at 1000 °C for 4 h in air, the targeted samples in form of white body (see **Figure 6(c)**) were achieved.

3.2 Phase, Morphology, Static and Dynamic Photoluminescence (PL) Characterizations

The Bruker D8 ADVANCE powder diffractometer (operating at 40 kV, 40 mA, and 1.2°·min^{-1}) with $Cu_{K\alpha}$ radiation (λ = 1.54059 Å) was used to examine the phase purity of all $ZnWO_4$:xBi^{3+} phosphors through X-ray diffraction (XRD). The composition characterization of the selected $ZnWO_4$:1.0%Bi^{3+} phosphor was performed by using the scanning electron microscopy (SEM, FEI Nova NanoSEM 430). The transmission electron microscopy (TEM) and high-resolution TEM (HRTEM) images of $ZnWO_4$:1.0%Bi^{3+} phosphor was recorded by the JEOL JEM-2100F instrument. The valence of Bi was checked by X-ray photoelectron spectroscopy (XPS), with the help of the Kratos Axis Ultra DLD spectrometer (Kratos Analytical Ltd., Wharfside, Manchester, UK) with a focused monochromatic $Al_{K\alpha}$ X-ray beam (1486.6 eV, 5 mA×10 kV, ~5×10^{-9} torr). The final binding energies were calibrated with the reference to the C1s peak at 284.8 eV. Photoluminescence (PL) spectra and fluorescence decay curves were measured in the 10-300 K temperature range with a high-resolution FLS 920 spectrofluorometer (Edinburgh Instruments), which is equipped with a thermoelectric cooled red-sensitive photomultiplier tube (Hamamatsu R928 P) in the single photon counting mode. The excitation source for PL spectra and the excitation photons for the fluorescence decay curves were a 450 W Xenon lamp and a 60 W μF900 flash lamp, respectively. All excitation and emission spectra were corrected over the lamp intensity with a silicon photodiode, and further normalized by the PMT spectral response.

4. RESULTS AND DISCUSSION

4.1 Analysis on Possible Types of Bi Doping through DFT Calculations

As previously mentioned, we could not confirm whether Bi^{3+} ions could readily substitute the Zn^{2+} and W^{6+} sites. Thus, the following possible types of Bi doping have been initially screened by the DFT calculations, aiming at excluding some impossible substitution prior to our experimental process and to find how the electronic properties of $ZnWO_4$ crystal change after Bi doping.

4.2.1 Consideration on Bi_{Zn} and Bi_W

Under O-rich or Zn-poor chemical potential limit, the formation energy for Bi_{Zn} and Bi_W at ground state (0K) is -1.55 eV and -0.38 eV per defect site. The two negative values mean that both Bi_{Zn} and Bi_W formation are rather energetically favorable and cost even less than the other native point defects formed in the host lattice. Clearly, the formation energy of Bi_{Zn} is lower than that of Bi_W, indicating the Bi_{Zn} has more stable energetic configuration with local lattice relaxation. Besides,

basing on the defect reactions of $2Bi_{Zn}^{2+} \rightarrow Bi_{Zn}^{+} + Bi_{Zn}^{3+}$ and $2Bi_{W}^{2+} \rightarrow Bi_{W}^{+} + Bi_{W}^{3+}$, both Bi_{Zn} and Bi_{W} have negative-U_{eff} effects and their values are -0.30 eV and -1.16 eV, respectively. This means the Bi_{Zn}^{2+} and Bi_{W}^{2+} are all unstable charge states and the life time in lattice will be rather short and, meanwhile, the charge state spontaneously undergoes the transition and re-distributes the charges into the single and triple positively charged doping state. In view of this, only 0, +1, and +3 charge states are stable valence for Bi substitution in the $ZnWO_4$ host lattice. Therefore, for Bi_{Zn} and Bi_{W} doping types, we screen the six possibilities through the DFT calculations, *i.e.*, the W-substituted Bi^0 (*i.e.*, Bi_{W}^{0}), W-substituted Bi^+ (*i.e.*, Bi_{W}^{+}), W-substituted Bi^{3+} (*i.e.*, Bi_{W}^{3+}), Zn-substituted Bi^0 (*i.e.*, Bi_{Zn}^{0}), Zn-substituted Bi^+ (*i.e.*, Bi_{Zn}^{+}), and Zn-substituted Bi^{3+} (*i.e.*, Bi_{Zn}^{3+}). The PDOS properties for Bi_{Zn} and Bi_{W} doing types have been depicted in **Figure 1**(**c-d**)(**i-iii**). In the figures, replacing the W site with different Bi valences seems do not change the band-gap sizes significantly (*i.e.*, the E_g value keeps at ~2.60 eV), and the O-2p and W-5d levels also contribute dominantly to VB and CB. For Zn-substituted Bi (**Figure 1**(**d**)(**i-iii**)), however, the band-gap size as the Bi decreases from high valence (+3) to low valences (+1 and 0) exhibits in sharp difference, *i.e.*, ~1.98 eV for Bi_{Zn}^{3+}, ~2.99 eV for Bi_{Zn}^{+}, and ~0.69 eV for Bi_{Zn}^{0}. PDOS results indicate us that the influence of Bi valence on Bi_{Zn} doping type is stronger than that of Bi_{W} type.

4.2.2 Consideration on Bi_i

Due to the sharp ionic radii between six-oxygen coordinated Zn, W and Bi ions and their valence difference, incorporating Bi into $ZnWO_4$ may also lead to generate the Bi interstitial doping (Bi_i) directly. However, our DFT calculations showed that the formation energy of Bi_i under the Bi-rich chemical potential limit is up to 7.83 eV, which illustrate that such formation is very unstable and needs more energy to form within the host lattice. If the Bi_i case did really exist in Bi doped $ZnWO_4$ crystal lattice, it would be a spontaneous process for Bi_i that transform into Bi_{Zn} or Bi_{W} via local migration to the nearest neighboring V_{Zn} or V_{W} site.

4.2.3 Consideration on Charge Compensated Complex

It has been well known that the physicochemical properties of perfect crystals can be interrupted significantly by crystal defects. Typically for the artificial crystal materials, some defects may induce the change in their physiochemical properties. For example, the defects allow MoS_2 to emit colorful emissions,[49] and exhibit the abnormal enhanced PL intensity in $LuVO_4:Bi^{3+}$ phosphor.[50] Considering the frequently used synthesis method for phosphors is the solid-state strategy and thus, crystal defects are inevitably avoided. As consequence, this drives us to consider the following two charge compensated complex.

If the Bi_{Zn} and Bi_{W} substitutions were involved simultaneously, the increasing probability of the Bi

substitution in the same cationic site may appear with the increase of the Bi doping content, which indicates us to focus on the effect of the local clustering on native point defects and dopants. Under DFT consideration, we initially suppose that the local short range disorder in the lattice will occur spontaneously because the local charge distribution needs to be balanced. When the Bi_{Zn} type is formed, the most stable valence charge state is Bi_{Zn}^{3+}, which is also used to the Bi_{W}^{3+} case. To compensate the 3+ charge, a $(1/2)V_{W}^{6-}$ (where V is denoted as vacancy) with opposite charge is formed in order to keep the local neutrality. Since this tends to be more energetically favorable, the Bi dopants have closer crossover distances in $ZnWO_4$ crystal lattice. In consequence, two charge compensated complexes, $2Bi_{Zn}V_{W}$ and $2Bi_{W}3V_{Zn}$, which derive respectively from the Bi_{Zn} and Bi_{W} doping types, are coming. Our results showed the formation energies for $2Bi_{Zn}V_{W}$ (*i.e.*, 0.95 eV) and $2Bi_{W}3V_{Zn}$ (*i.e.*, 9.95 eV) are sharply different from each other and, based on the two values, the latter type is more difficult to form than the former. More remarkable, comparing the PDOS properties of **Figure 1**(**c**)(**iv**) and **Figure 1**(**d**)(**iv**) with respective that of **Figure 1**(**c**)(**i-iii**) and **Figure 1**(**d**)(**i-iii**) reveals the orbital levels that dominantly contribute to VB and CB does not change. In the figures, the band-gap (~1.93 eV) for $2Bi_{W}3V_{Zn}$ (**Figure 1**(**c**)(**iv**)) coincides basically with that (~2.20 eV) without considering the crystal defect(**Figure 1**(**c**)(**i-ii**)), but the band-gap (1.00 eV) for $2Bi_{Zn}V_{W}$ (**Figure 1**(**d**)(**iv**)) is 1.98 times, 2.69 times and 0.69 times less than that of ~1.98 eV for Bi_{Zn}^{3+} (**Figure 1**(**d**)(**iii**)), ~2.69 eV for Bi_{Zn}^{+} (**Figure 1**(**d**)(**ii**)) and ~0.69 eV for Bi_{Zn}^{0} (**Figure 1**(**d**)(**i**)). Due to the large difference of ions radii and valence between W and Bi, the PDOS properties for $2Bi_{W}3V_{Zn}$ should change as compared to that of bulk $ZnWO_4$, but DFT results show the situation is not like this. Doping Bi into Zn sites always allows the PDOS properties changing more significant than W sites compared to bulk $ZnWO_4$. Moreover, if Bi could substitute for W site, the formation energy should be relative low, but we see that the value (9.95 eV) is very high. This illustrates from the other side that doping W site with Bi ion seems impossible in Bi doped $ZnWO_4$ crystal.

4.2.4 Discussion on Reaction-Decomposition Reaction in $ZnWO_4$ Crystal

In the $ZnWO_4$ formation process, it experiences a series of reversible reaction-decomposition reactions (*i.e.*, $ZnO + WO_3 \rightleftharpoons ZnWO_4 \rightleftharpoons ZnO + WO_3$). When the conventional high temperature solid-state reaction is used as the synthesis method, this process will become more prominent. Typically, when the temperature is over 1100 K, the ZnO compounds trend to decompose into the O_2 and Zn vapor gas easily. Hence, we calculated the formation enthalpies for ZnO, WO_3 and $ZnWO_4$ (-15.47 eV) compounds, and results show their values are -3.67 eV, -10.80 eV and -15.47 eV, respectively. Obviously, these values are in a large contrast, typically between the ZnO and $ZnWO_4$. According to similar theoretical works reported by Huang *et al* in CaZnOS crystal[51], the

vacancy formation of the ZnO local motif (V_{ZnO}) costs rather low energy. In view of this, formation of ZnO vacancy (V_{ZnO}) within the $ZnWO_4$ host lattice seems possible. On basis of V_{ZnO} formation energy within charge states of 0, -1, -2, +1 and +2, the V_{ZnO} is a negative-U_{eff} effect in the defect reaction of $2V_{ZnO}^{+} \rightarrow V_{ZnO}^{0} + V_{ZnO}^{2+}$ and the rest of charge state transition shows the positive-U_{eff} effects, indicating that the most stable charge states for V_{ZnO} are 0, -1, -2, and +2.

4.3 Analysis on Potential Modulation of the Output Luminescence

Although there are so many Bi doping possibilities as screened by the DFT calculations, questions are still remaining. Whether all of these possibilities could work for the output luminescence in Bi doped $ZnWO_4$ crystal and allow Bi emitting the required luminescence that can address the sticky problems as mentioned in "**1.INTRODUCTION**" section? It would be highly desirable, if we could find some clues ahead of the experiment through the DFT calculations.

According to the analysis from DFT results, we could deduce that the most possible doping types that could induce the output luminescence in $ZnWO_4$:Bi crystal are Bi_{Zn} (including Bi_{Zn}^{3+}, Bi_{Zn}^{+}, and Bi_{Zn}^{0}), $2Bi_{Zn}V_W$ and V_{ZnO} (including V_{ZnO}^{0}, V_{ZnO}^{-}, V_{ZnO}^{2-}, and V_{ZnO}^{2+}) and, based on them, single-particle levels (SPLs) are draw, as depicted in **Figure 1**(**e**). Depending on the charge states, there are two emission parts for Bi_{Zn} doping type. One locates within the $ZnWO_4$ host that gives medium wavelength within 600~700 nm range, and another one is near infra-red (NIR) emissions which derive from the transitions between the localized electronic and hole levels within the optical fundamental band gap area. For the defect complex model of $2Bi_{Zn}V_W$, it exhibits a wide range of emission wavelengths from 500 nm to 827 nm, which precisely cover all Bi_{Zn} emissions. As for V_{ZnO} emissions, except for V_{ZnO}^{-}, others are all having the potency in emitting NIR light, i.e., 700 nm for V_{ZnO}^{0}, 785 nm for V_{ZnO}^{2+}, and 704 nm for V_{ZnO}^{2-}. From **Figure 1**(**e**), emissions in $ZnWO_4$:Bi crystal are very complicated and there are so many possible interaction, typically those having close emission wavelengths, *e.g.*, 500 nm (green) for both $2Bi_{Zn}V_W$ and V_{ZnO}^{0}, and 512 nm (green) for Bi_{Zn}^{2+}. In consequence, this wide emission range in $ZnWO_4$:Bi enables pumping tunable luminescence upon a fixed excitation wavelength and/or through controlling external condition such as the temperature and the doping content. More importantly, due to the potential existence of red luminescence in the figure through the DFT prediction, for example, 611 nm and 629 nm for V_{Bi}^{3+}, novel red Bi^{3+} luminescence that is noticed by previous works may appear in $ZnWO_4$:Bi crystal. However, relying on the DFT results, we find that to precisely predict the PL properties of $ZnWO_4$:Bi^{3+} phosphor is strongly far from enough. Since the DFT calculations are constructed under a relative ideal condition, results predicted by DFT calculations sometimes do not mean that they can be achieved by the experiment, typically when a complicated synthesis is involved by the

experiment and, thus, we design the experiment to verify the DFT prediction.

4.4 Experimental Confirmation

4.4.1 Structural Analysis

To check the influence of Bi doping on the phase purity and micro-structural morphology, we measured the XRD and SEM patterns of $ZnWO_4$ crystal with and without Bi doping, as shown in **Figure 2**(**a**) and **Figure 2**(**c-f**), respectively. It clearly shows from **Figure 2**(**a**) that all diffraction lines coincide with the $ZnWO_4$ standard pattern (No. 1520641) derived from the Inorganic Crystal Structure Database (ICSD), indicating incorporating Bi into the $ZnWO_4$ lattice does not induce the detectable impure phase. All samples crystallize in the targeted monoclinic wolframite-type structure with the space group *P*12/*c*1 (No. 13). However, a closer inspection into the XRD results reveals that the diffraction intensity distribution for Bi^{3+} doped samples is quite different from that of the $ZnWO_4$ standard pattern and bulk $ZnWO_4$ crystal. As denoted by "♀"and "♂" for the planes (-111), (111) and (020), the relative diffraction intensities of (-111) and (111) planes for bulk $ZnWO_4$ crystal are stronger than that of (020) plane. While the diffraction curves from 0.5%Bi content to 3.0%Bi content show that Bi doping has reversed this situation, the relative diffraction intensity of (-111) and (111) planes becomes abnormally weaker than that of (020) plane. Other diffraction planes (011) and (110), (022) and (200) also reflect such change. However, the relative diffraction intensities between different planes as the Bi content increases remain similar, indicating they are independent of Bi content. As a result, increasing Bi content does not change the morphologies, as confirmed by SEM images (**Figure 2**(**c-f**). With this information, we deduce that doping Bi not only enables enlarging the particle size, but also tuning the irregular spheroidicity (for bulk $ZnWO_4$) into the quadrangular prism (for $ZnWO_4$:Bi).

To illustrate the above change more clearly, high-resolution TEM (HRTEM) technique with the Fast Fourier Transform (FFT) pattern was employed to measure the thinnest fringe of one selected $ZnWO_4$:1.0%Bi^{3+} particle, as depicted in **Figure 2**(**g-h**). Clearly, two different interplanar lattice distances of 0.487 nm and 0.285 nm, which precisely correspond respectively to the (020) and (100) lattice planes of $ZnWO_4$ crystal with the monoclinic wolframite-type phase, appear in the sample. Our energy-dispersive X-ray (EDX) spectroscopy confirms that the particle contains the Zn, W, O and Bi elements (**Figure 2**(**b**)), which, together with the lack of the crystallization anisotropy in bulk $ZnWO_4$, indicates that doping Bi has induced the anisotropic growth problem. Additionally, results of **Figure 2** also reveal the anisotropic grain and the crystallization process of Bi doped $ZnWO_4$ samples are grown along *c*-axis, with the orientation along the (0k0) and (h00) planes. These results tell us from the other side that incorporation of Bi, as previously predicted by the above DFT

analysis, really has caused great influence on the structural behavior, thereby leading to the following experimentally spectral observations.

4.4.2 Room-Temperature Spectral Analysis

Upon monitoring at the wavelength of 665 nm, the room-temperature excitation spectra shown in **Figure 3**(**a**) for Bi doped $ZnWO_4$ phosphors exhibit two overlapping broad excitation bands at 295 nm and 365 nm, which, in combination with the excitation wavelength of **Figure 3**(**b**), are assigned to the absorption of host and Bi activator, respectively. When we turn the monitored emission wavelength into 485 nm (**Figure 3**(**b**)), Bi doped phosphors exhibit only one broad band at 295 nm (**curve 1**-**6**), which is very similar to bulk $ZnWO_4$ phosphor (**curve 0**). The energy calculated from the maximum excitation intensity (~4.203 eV) of bulk $ZnWO_4$, agrees well with the E_g value (~4.019 eV) as calculated by DFT (**Figure 1**(**b**)). Unlike the bulk $ZnWO_4$ excitation tail terminated at ~350 nm, all Bi doped phosphors upon monitoring at 665 nm show the tail at 425 nm (**Figure 3**(**a**)), suggesting they can only be excited by near-UV light rather than visible light. This matches well with commercial UV LED chip with the emission wavelength of 380~420 nm and, because of the non-excitation in visible region, can address well the sticky visible light reabsorption problem that encounters in such Eu^{2+}, Ce^{3+}, Mn^{2+}, Mn^{4+} and Cr^{3+} activators. As depicted in **Figure 3**(**c**), upon excitation at 365 nm enables Bi doped phosphors to exhibit red emissions, and the maximum emission position as the Bi doping content increases blue-shifts slightly from 666 nm for $ZnWO_4$:0.5%Bi to 658 nm for $ZnWO_4$:3.0%Bi. However, when exciting these samples at the absorption range of bulk $ZnWO_4$ (~305 nm), with increasing the Bi content, a red-shift of emission position, starting from 485 nm for bulk $ZnWO_4$ phosphor, appears. The emission position for the maximum Bi doping (3.0%) is locating at 489 nm (see **Figure 3**(**d**)).

With the spectral results of **Figure 3**(**a**-**d**), some unusual yet interesting results have been also shown, *i.e.*, the Bi content, which corresponds respectively to the maximum excitation intensity of host and Bi, is strongly depending on the monitored emission wavelength. Typically, monitoring at the wavelength of 665 nm allows Bi doped phosphors exhibiting the optimal Bi content of 0.5% and 1.0% for the maximum excitation intensity of host (~295 nm) and Bi dopant (~365 nm), respectively (see **Figure 3**(**a**)), nevertheless, upon excitation at 365 nm, the Bi doping content for the maximum emission intensity is 0.5%. Hence, the emergence of the inconsistence between the Bi excitation intensity and the corresponding emission intensity can be understood. However, no matter which host absorption and emission wavelengths are selected to excite or monitor the Bi doped phosphors (**Figure 3**(**b**) and **Figure 3**(**d**)), the spectral intensity of Bi doped samples decreases with increasing Bi content, and all Bi doped phosphors show the spectral intensity lower than bulk $ZnWO_4$ phosphor.

This hints that there probably exists a kind of forward and backward energy transfer between host and Bi dopant and, such interaction is sensitive to the Bi content.

Nominally, the emission position does not change with the change of Bi doping content if there is only one luminescence site in the crystal lattice. As implied by DFT results, however, the types, Bi_{Zn}, $2Bi_{Zn}V_W$ and V_{ZnO}, are the most possible types for generating the output luminescence in $ZnWO_4$:Bi phosphor. If they were all involved, tunable emissions as the Bi content changes, therefore, are reasonable. Accordingly, the emission position as the excitation wavelength changes should also changes regularly, because the emissions for different doping types predicted by DFT calculations show different energies. Thus, we also measured the excitation-dependent spectra for all Bi doped phosphors, as shown in **Figure 3**(**e-f**). In **Figure 3**(**e**), decreasing the excitation from 250 nm to 420 nm really has trigged the $ZnWO_4$:1.0%Bi phosphor to tune the emission positions from 485 nm (*i.e.*, bulk $ZnWO_4$ emission) to 665 nm (*i.e.*, Bi emission), following by a slight red-shift of $ZnWO_4$ emission position and an initial red-shift with a subsequent blue-shift for Bi emission position. Such excitation-dependent emission position keeps the same tendency as the Bi doping content increases (**Figure 3**(**f**)). All emission positions upon excitation from 330 nm to 340 nm show a suddenly direct jump into Bi emission, without appearing the regular emission position transition as expected. As depicted by many previous works, some spectral information which can only be observed at room temperature may change as the temperature changes, typically when the temperature is close to the ground state (0K), for example, alternation of predominant emissions between VO_4^{3-} groups and Bi^{3+} in Bi^{3+} doped vanadates,[27] shifting of multiple emissions toward different directions, *e.g.*, ZnO,[52] $CaMoO_4$:Bi,[53] $CaWO_4$:Bi,[54] and $La_2Zr_2O_7$:Bi^{3+}.[55] Returning to the emissions resulting respectively from Bi_{Zn}, $2Bi_{Zn}V_W$ and V_{ZnO} doping types (**Figure 1**(**e**)), there are a wide range of emissions from green light to NIR light, but most of them seem have been hidden at room temperature and, thus, we measured the following temperature dependent PL spectra for $ZnWO_4$:Bi phosphor, expecting to find some individual yet tight PL interaction that cannot be observed at room temperature.

4.4.3 Influence of Temperature on PL Spectra and Decay Dynamics

Figure 4(**a**-**e**) give the excitation and emission spectra of $ZnWO_4$:1.0%Bi phosphor measured within10-300 K temperature range. Unlike PL spectra at room temperature, gradually increasing the monitored emission wavelength from 450 nm to 700 nm keeps the excitation spectral sharp (**Figure 4**(**a**)). All excitation tails also terminate at 425 nm, which are similar to that of **Figure 3**(**a**). However, the excitation intensity distribution, in particular the band centering at ~365 nm, exhibits differently. With defining the maximum excitation intensity of host as the normalized intensity, the Bi intensity

as the monitored emission wavelength increases appears gradually, followed by a slight red-shifting position. In addition, the Bi doped $ZnWO_4$ phosphor at low temperature (10 K) (close to the ground state temperature of 0 K) features a sharply different PL behavior compared to that at room temperature. As the excitation wavelength changes from 250 nm (for $ZnWO_4$ host) to 380 nm (for Bi dopant), the dominant emission position at 10 K red-shifts gradually from 498 nm to 650 nm (**Figure 4**(**b**)). In sharp contrast, as temperature increases from 10 K to 300 K, upon excitation at the wavelengths of 270 nm (*i.e.*, the host excitation), 360 nm (*i.e.*, the Bi excitation) and 310 nm (*i.e.*, the excitation boundary between host and Bi dopant) enables the $ZnWO_4$:Bi phosphor to regularly exhibit tunable emissions, differing in the emissions at room temperature (**Figure 3**(**e-f**)) and at 10 K (**Figure 4**(**a-b**)). In **Figure 4**(**c**), the emission peaks achieved by exciting at 270 nm only move towards shorter wavelengths from 498 nm at 10 K to 485 nm at 300 K, but exciting at 360 nm red-shifts the emission peaks from 625 nm at 10 K to 680 nm for 150 K and then back to 655 nm at 300 K (**Figure 4**(**d**)). Comparing the emission spectra between **Figure 4**(**c**) and **Figure 4**(**d**) illustrates that the latter exhibits the tunable range larger than the former. Moreover, **Figure 4**(**c**) shows an emission band beyond 575 nm (> 575 nm), which appears gradually with increasing the temperature (see the rectangular frame).

To illustrate the influence of Bi doping on dynamic PL results, we simultaneously measured the decay curves for bulk $ZnWO_4$ and $ZnWO_4$:1.0%Bi phosphors within the temperature range of 10-300 K, as shown in **Figure 5**(**a-b**). The excitation wavelength and the monitored emission wavelength are 305 nm and 485 nm, corresponding to the absorption region and the maximum emission intensity of bulk $ZnWO_4$ crystal, respectively. For bulk $ZnWO_4$ crystal, the decay dynamic behaviors do not change with the increase of temperature, keeping a single-exponential decay. Fitting into the decay curves with single-exponential equation of $I = A\exp(-t/\tau)$ (where parameters A, I and t are the fitted constant, the luminescence intensity and the decay time, respectively) enables achieving a series of host lifetime values. As depicted by **Table 1** and **Figure 5**(**c**)(black curve), the emission lifetimes of bulk $ZnWO_4$ crystal as the temperature increases drop gradually from 46.99 μs to 34.62 μs. For Bi^{3+} doped $ZnWO_4$ crystal, however, it exhibits double-exponential decay behavior when temperature is below 100 K. With the second-order exponential equation described as $I = A_1\exp(-t/\tau_1) + A_2\exp(-t/\tau_2)$ (where I is the luminescence intensity; τ is the average decay time; A_1 and A_2 are constants; t is the time; and τ_1 and τ_2 are rapid and slow lifetimes for exponential components), the decay curves can be fitted, and further calculation into the two series of values by using the equation of $\tau_{ave} = (A_1\tau_1^2 + A_2\tau_2^2)/(A_1\tau_1 + A_2\tau_2)$ enables obtaining the average emission lifetimes (**Table 1** and **Figure 5**(**c**)(red curve)). As temperature exceeds 100 K, the decay for

$ZnWO_4$:Bi phosphor is a single-exponential decay, and it does not change with further increasing temperature. Bi doped phosphor experiences a different decay compared to bulk $ZnWO_4$ crystal.

4.5 Discussion on Spectrally Tunable Observation

In **Figure 4(f)**, we find the $ZnWO_4$:1.0%Bi phosphor shows two characteristic XPS peaks at 159.3 eV and 164.6 eV due to ${}^4f_{7/2}$ and ${}^4f_{5/2}$, which match well with peaks of α-Bi_2O_3, implying the bismuth valence in $ZnWO_4$:1.0%Bi phosphor is +3 and belongs to on potential bismuth valence predicted by DFT calculations. Previous works on Bi^{3+} decay curves reveal that the two ${}^1S_0 \rightarrow {}^3P_1$ and ${}^3P_0 \rightarrow {}^1S_0$ emission transitions that determine the nature of Bi^{3+} lifetime are strongly dependent on the temperature.[36, 53, 54] Since the ${}^3P_1 \rightarrow {}^1S_0$ transition is *Laporte* allowed, the decay time usually spans between 10^{-6} and 10^{-8} s.[36] While the ${}^3P_0 \rightarrow {}^1S_0$ transition is a spin forbidden transition, allowing it can be only pumped by low temperature and thus, the corresponding emission lifetime frequently exhibit several hundred microseconds.[53, 54] Hence, controlling the temperature enables controlling the population redistribution between ${}^3P_0$ and ${}^3P_1$ levels. Because of this behavior, yellow $LuVO_4$:Bi^{3+} and red $ScVO_4$:Bi^{3+} phosphors as the temperature increases from 10 K to 300 K and even to 500 K experiences a decay process from double-exponential to single exponential decay behavior,[28, 29] and their Bi^{3+} lifetimes at high temperature (*i.e.*, >250 K) only exhibit several microseconds and even several hundred nanoseconds. For the decay behavior, the $ZnWO_4$:Bi phosphor experiences a similar process, but the fitted lifetimes, as depicted by **Table 1** and **Figure 5**, are obviously much greater than that of $LuVO_4$:Bi^{3+} and red $ScVO_4$:Bi^{3+}, typically when the temperature is higher 250 K. In view of this, we, therefore, deduce the emission position of 485 nm and the excitation position of 305 nm do not involve the Bi^{3+} counterparts, and some vital but infrequently-noticed factors have played the key role in modulating the output Bi^{3+} luminescence in $ZnWO_4$:Bi^{3+} crystal.

With the experimental PL results of **Figure 3** and **Figure 4**, the Bi_{Zn}^{+} (738 nm) or V_{ZnO}^{2+} (785 nm) emissions predicted by **Figure 1(e)** should not contribute to the experimental PL emissions, since, no matter at room temperature or low temperature, they cannot be detected individually. The 484 nm emission from V_{ZnO}^{2+} doping type may contribute to the blue emission of **Figure 3(c)**. In view of the emission bands in bulk $ZnWO_4$ sample (**Figure 6(a)**) and Bi^{3+} doped $ZnWO_4$ sample (**Figure 4(c)** and **Figure 4(e)**), it is possible for V_{ZnO}^{0} (700 nm), V_{ZnO}^{-} (629 nm, and 611 nm) and V_{ZnO}^{2+} emissions (704 nm) to contribute, and the experimental emission bands has obviously covered all V_{ZnO} emissions. In addition, the alteration emission intensity shown in **Figure 6(a)** reveals that the emission band 700 nm is from V_{ZnO}^{0} and V_{ZnO}^{2+} emissions, and they are strongly dependent on the temperature. In this case, they can contribute to the emission at low temperature

and, at the same time, modulate the emission position at high temperature. When compared to the Bi_{Zn} doping type, the formation energy for the neutral state of V_{ZnO}^{0} under the O-rich chemical potential limit is 2.47 eV, indicating the V_{ZnO}^{0} at room temperature has a relatively lower priority than the Bi substitution in Bi^{3+} doped $ZnWO_4$ crystal. Thus, the V_{ZnO}^{0} type has nothing to do with Bi^{3+} doping, and it just comes from bulk $ZnWO_4$ crystal. Except for the V_{ZnO}^{0} emission itself, the main contribution of V_{ZnO}^{0} in Bi^{3+} doped $ZnWO_4$ crystal is to act as the intermediate energy transfer path to broaden and tune the emission wavelength. As for the case of $2Bi_{Zn}3V_W$, the emission wavelength of 827 nm that exceeds our measurement range, but others emissions (*i.e.*, 500 nm, 534 nm and 660 nm), which agree well with our experimental green and red emission bands, are involved. If we could not consider the doping defect, the actual emissions of Bi_{Zn}^{3+} type are located at 611 nm and 629 nm and, thus, they are impossible to contribute to the experimental 665 nm emission of Bi^{3+} at room temperature. However, they may appear at low temperature, in view of the regular emission positions with pumping by different excitation wavelengths at low temperature (**Figure 4**). This is similar to the case of Bi_{Zn}^{0} type. The ordered $ZnWO_4$ crystal lattice has only one crystallographic site for tungsten and zinc atom, but we assume that the experimental results reflect a slight deviation from the ideal structure, in view of the DFT and experimental results. From the PL spectra, the emissions and excitations are not only strongly dependent on temperature, but also Bi doping content and the monitored energy. To systematically illustrate the above analysis, a complicated but feasible diagram for experimental PL observation in $ZnWO_4$ crystal and $ZnWO_4$:Bi is draw, as depicted in **Figure 6**(**b**).

In bulk $ZnWO_4$, exciting at the host absorption leads to the host blue-green emission (*i.e.*, 495 nm) at 10 K and, due to the gradual emergence of 484 nm from V_{ZnO}^{2+} emission with the increase of temperature, this host emission band shifts to 484 nm at 300 K. In the meanwhile, since the 512 nm emission from V_{ZnO}^{2+} is also involved, the broadened host emission band, which results from the increase of temperature, is reasonable. Note that only the typical 495 nm emission has been given in the figure. Similarly, with the increase of temperature, the 700 nm and 704 nm emissions that come respectively from V_{ZnO}^{0} and V_{ZnO}^{2-}, which only appears at low temperature, quenches gradually and, due to the possible thermal perturbation, changing the temperature enables slightly tuning this emissions band.

In Bi^{3+} doped $ZnWO_4$ phosphor, since there is a large overlap of the excitation band Bi^{3+} activator and the emission band of $ZnWO_4$ host (**Figure 3**(**a**) and **Figure 3**(**d**)), simultaneous Bi^{3+} and $ZnWO_4$ emissions upon excitation with the absorption wavelength of $ZnWO_4$ host (*e.g.*, 325 nm) are understood, indicating there is an energy transfer from $ZnWO_4$ host to Bi^{3+}. However, upon

excitation at Bi^{3+} only induces the Bi^{3+} emission (**Figure 4(d)**), without the $ZnWO_4$ emission, implying the energy transfer is unidirectional and the emissions of $ZnWO_4$ host and Bi^{3+} do not influence each other. With the increase of temperature (**Figure 4(c)**), the blueshift of emission position upon excitation at 270 nm can be interpreted by the gradual alteration from $ZnWO_4$ host emission to V_{ZnO}^{2+} (484 nm), similar to the situation of bulk $ZnWO_4$ crystal. However, the emergence of emission within the rectangle (**Figure 4(c)**) indicates the increase of the energy transfer from $ZnWO_4$ host to Bi^{3+} with the increase of temperature. More than that, when the excitation wavelength is changed into 310 nm (closer to Bi^{3+} excitation band), the energy transfer efficiency from $ZnWO_4$ host to Bi^{3+} becomes more efficiency at low temperature than that upon excitation at 270 nm, and it decreases with increasing the temperature. As a result, only $ZnWO_4$ emission upon excitation at 310 nm appears at room temperature. Owning to the contributions on emissions from other doping types (*i.e.*, 629 nm and 611 nm for V_{ZnO}^{-}, 544 nm for V_{ZnO}^{2-}, 512 nm for V_{ZnO}^{2+}, 579 nm for Bi_{Zn}^{0}, 611 nm and 629 nm for Bi_{Zn}^{3+}, 500 nm and 534 nm for $2Bi_{Zn}3V_W$) and their manageable energy interactions, tunable emissions in $ZnWO_4$:Bi phosphor is observed. However, we can know from experimental PL results that not all emissions appear once and for all. some emissions emerge only at a certain temperature and/or a fixed excitation wavelength. In this case, interaction between different emissions could also appear. In **Figure 6(b)**, the role of Bi doping types can be divided into: (i) Bi_{Zn}^{0}, V_{ZnO}^{-} and V_{ZnO}^{2-} as well as $2Bi_{Zn}3V_W$ for tuning and broadening the low temperature emission from green to red; (ii)V_{ZnO}^{2+} for pumping and tuning the green emission ranging from 512 nm to 484 nm; (iii) V_{ZnO}^{0} and V_{ZnO}^{2-} for generating and tuning the 700 nm NIR emission and, at the time, broadening the Bi^{3+} emission, though they cannot be reflected in $ZnWO_4$:Bi crystal. Additionally, due to the emission energy difference from these doping types, the manageable interactions, which depend on the temperature and excitation wavelengths, appears, according to our experimental PL results. As a consequence, we achieve the phosphor with a visible color tuning from green to red (**Figure 6(c)**). Typically, no matter how the situation changes, this $ZnWO_4$:Bi phosphor only allows the excitation tail terminating to 425 nm, which shows the potency in addressing the visible light reabsorption problem.

4.6 Design Concept for Novel Bi^{3+} Red Luminescence

As we have mentioned in "**1. INTRODUCTION**" section, Bi^{3+} features a host-sensitive behavior and, thus, it can exhibit different emission positions in different crystals. Comparing the red emission position (~665 nm) of the $ZnWO_4$:Bi red phosphor with that (~635 nm) of $ScVO_4$:Bi^{3+} reveals that the red emission also depends on the crystal host, but the position for the former emission is longer than that of the latter. For the reason, we can explain it by using the dielectric

chemical bond theory, in which the spectral positions are dominantly influenced by the covalency (f_c) of the chemical bonds that connect the central Bi^{3+} ion and its oxygen ligands.[56] The larger covalency means the longer wavelength emission. For the red emissions, our DFT findings have indicated that they tend to come from the substitution of Zn^{2+} sites by Bi^{3+} ions. In view of this, we calculated the covalency f_c for each Zn-O bond (see **Table 2**), and results reveal the average covalency (f_c=0.3609) of Zn-O bond for $ZnWO_4$ crystal is much larger than that (f_c=0.1591) of Sc-O bond for $ScVO_4$ crystal,[29] which explain well their emission wavelength differences.

On basis of the production conditions of Bi^{3+} red emission in $ZnWO_4$ and $ScVO_4$ crystals,[33] we can find that crystal site available for Bi^{3+} doping is necessary, but it seems not enough to achieve the Bi^{3+} red emission, because Bi^{3+} usually emits only the color from UV to yellow, as predicted by DFT results and low temperature PL results. For Bi^{3+} red luminescence, discussions on DFT and PL results reveal that a crystal matrix that benefit the oxygen vacancies generation is more important, since these vacancies could reduce the total energy of the host and play the key role in modulating the Bi^{3+} luminescence toward lower energy direction (**Figure 6(c)**). In this case, the Bi^{3+} red luminescence should be due to the combined contributions of the complexes produced by Bi^{3+} doping and the corresponding oxygen vacancy induced by the replacement of crystal site with Bi^{3+}. More than that, as depicted by the electron clouds shown in **Figure 6(d)**, manageable substitution sites, which are sensitive to the change of the surrounding environment (typically the crystal defects that accompany with the doping process), are also required.

5. CONCLUSIONS AND OUTLOOK

In this work, we employed the DFT calculations to guide us to successfully discover a novel Bi^{3+} red luminescence in $ZnWO_4$:Bi^{3+} phosphor, which enables generating the excitation wavelength less 420 nm and thus showing the non-reabsorption in the visible region. More specifically, all possible types of Bi doping, including W-substituted (Bi_W), Zn-substituted (Bi_{Zn}), interstitial (Bi_i) and the charge compensated complexes ($2Bi_{Zn}V_W$ and $2Bi_W3V_{Zn}$), had been initially screened by employing the DFT calculations. In the experiment, upon excitation at 360 nm, we observed the emission peak of $ZnWO_4$:1.0%Bi^{3+} phosphor initially red-shifted from 626 nm to 688 nm and then blue-shifted back 654 nm as the temperature increased from 10 K to 300 K. This tunable emission strongly differed in the blue-shifting emission peak (from 500 nm to 484 nm) upon excitation at 270 nm. Additionally, we found the emission peaks of $ZnWO_4$:Bi^{3+} phosphors were dependent on the Bi doping content and the excitation wavelength as well as the temperature. For $ZnWO_4$:Bi^{3+} excitation spectra, w manipulating the temperature and the monitored emission energy enabled controlling the intensity distribution over the whole near-UV spectral region. These tunable PL observations,

together with DFT results, revealed the transferable energy hopping from host to the Bi_{Zn} sites and, with the crystal defects perturbation, the Bi^{3+} red luminescence eventually. As shown by this work, if the DFT prediction strategy could be extended to screen some impossible crystal host before the experiment, a large number of extra works that accompany with using the trial and error method can be reduced, thereby facilitating to discover the possible crystal host that can allow Bi^{3+} emitting red luminescence. Therefore, this work not only enables providing a forward-looking insight into exploring more crystal compounds which allow Bi emitting red light only upon the excitation of near-UV light to address the issues as mentioned in "**ABSTRACT**" and "**1.INTRODUCTION**", but also deepening the complicated interactions between Bi^{3+} ions and host lattice as well as broadening this feasible DFT strategy for researchers to reveal some undiscovered new luminescence properties behind other systems, exemplarily based on Eu^{2+}, Ce^{3+}, Tb^{3+}, Eu^{3+}, Sm^{3+}, Mn^{2+}, Mn^{4+} and Cr^{3+} doping.

ACKNOWLEDGEMENT

Financial supports are acknowledged from the Key Program of Guangzhou Scientific Research Special Project (Grant No. 201607020009), the National Natural Science Foundation of China (Grant No. 51672085), the Department of Education of Guangdong Province (Grant No. 2013gjhz0001), Fundamental Research Funds for the Central Universities, the Hundred, Thousand and Ten Thousand Leading Talent Project in Guangdong Program for Special Support of Eminent Professionals. Jin Han strongly thanks Dr. Fengwen Kang for assistance in revising this work, and also thanks Dr. Bolong Huang for offering the DFT calculations to support the experiment.

Table 1 Decay Lifetime of $ZnWO_4$:$x$$Bi^{3+}$ (x=0, 1.0%) Phosphors at 10-300 K (λ_{ex} = 305 nm, λ_{em} = 485 nm)

Temperature	x=0		x = 1.0%				
T /K	A	τ /μs	A_1	τ_1 /μs	A_2	τ_2 /μs	τ_{ave} /μs

10	0.8216	46.99	0.3915	2.63	1.967	37.01	30.87
50	0.8293	45.86	0.6227	1.48	0.5952	36.06	34.63
100	0.8372	44.13	0.4611	35.54	0.4611	35.54	35.54
150	0.8454	44.64	0.5004	38.85	0.5004	38.85	38.85
200	0.8468	44.29	0.5001	40.11	0.5001	40.11	40.11
250	0.8803	41.38	0.5001	39.48	0.5001	39.48	39.48
300	0.9523	34.62	0.5004	26.12	0.5004	26.12	26.12

Table 2 Bond Length *d* and Calculated Chemical Bond Covalency f_c for the Zn Site in $ZnWO_4$ and the Sc Site in $ScVO_4$

Compounds	Bond	Bond Length *d*(Å)	f_c
$ZnWO_4$ (ICSD #1520641)	Zn–O(1) × 2	1.9801	0.3711
	Zn–O(2) × 2	2.1072	0.3601
	Zn–O(2) × 2	2.2227	0.3516
	Average	2.1033	0.3609
$ScVO_4$ (ICSD # 78073)	Sc–O(1) × 4	2.1289	0.1634
	Sc–O(2) × 4	2.3672	0.1549
	Average	2.2481	0.1591

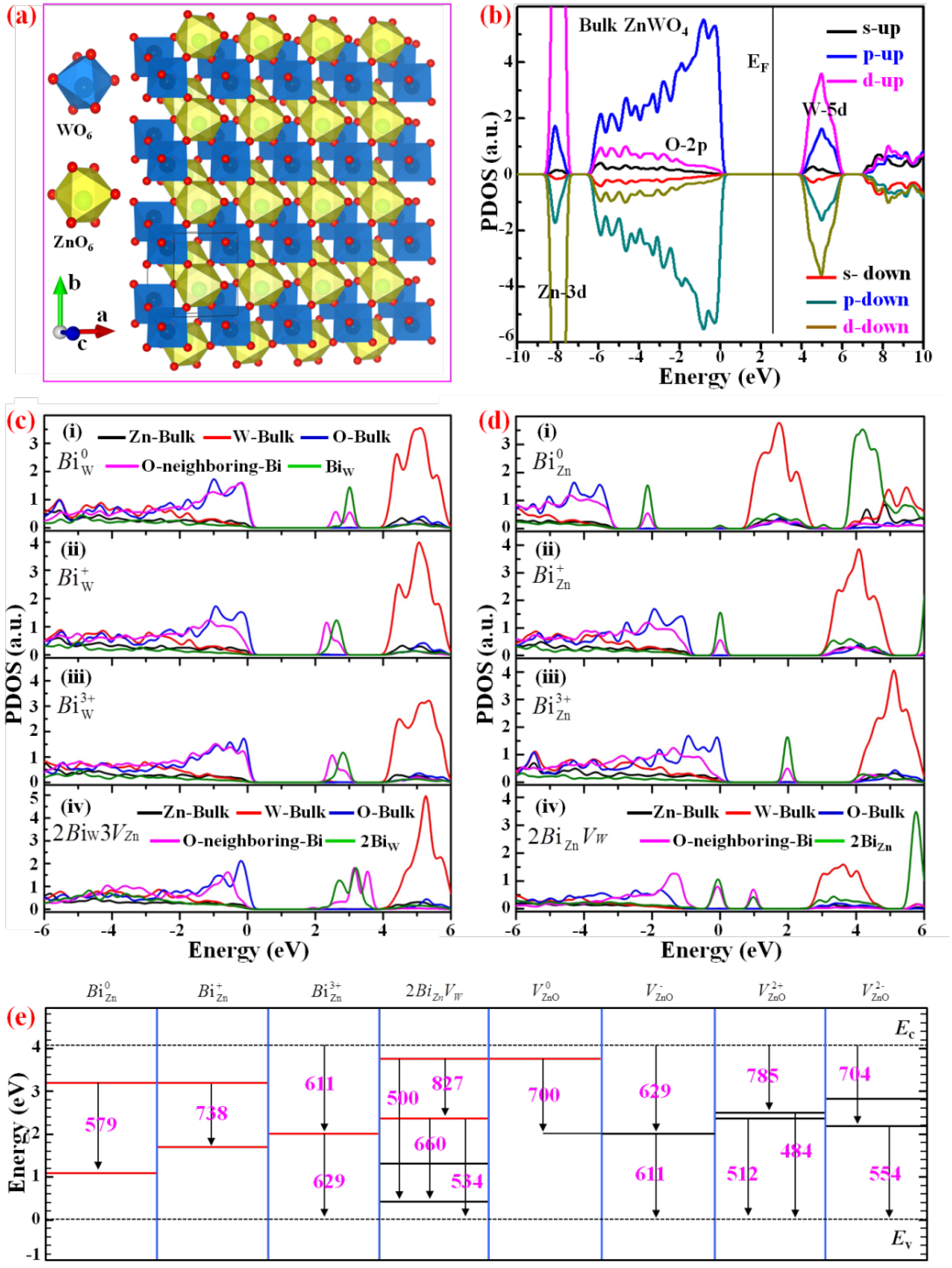
(a)
WO6
ZnO6
b
a
c
(b)
Bulk ZnWO4
EF
s-up
p-up
d-up
W-5d
O-2p
Zn-3d
s- down
p-down
d-down
PDOS (a.u.)
Energy (eV)
(c)
(i) Zn-Bulk W-Bulk O-Bulk
Bi0W O-neighboring-Bi BiW
(ii) Bi+W
(iii) Bi3+W
(iv) 2BiW3VZn
Zn-Bulk W-Bulk O-Bulk
O-neighboring-Bi 2BiW
PDOS (a.u.)
Energy (eV)
(d)
(i) Bi0Zn
(ii) Bi+Zn
(iii) Bi3+Zn
(iv) 2BiZnVW
Zn-Bulk W-Bulk O-Bulk
O-neighboring-Bi 2BiZn
PDOS (a.u.)
Energy (eV)
(e)
Bi0Zn
Bi+Zn
Bi3+Zn
2BiZnVW
V0ZnO
V-ZnO
V2+ZnO
V2-ZnO
Ec
Ev
Energy (eV)
579
738
611
629
500
827
660
534
700
629
611
785
512
484
704
554

Figure 1

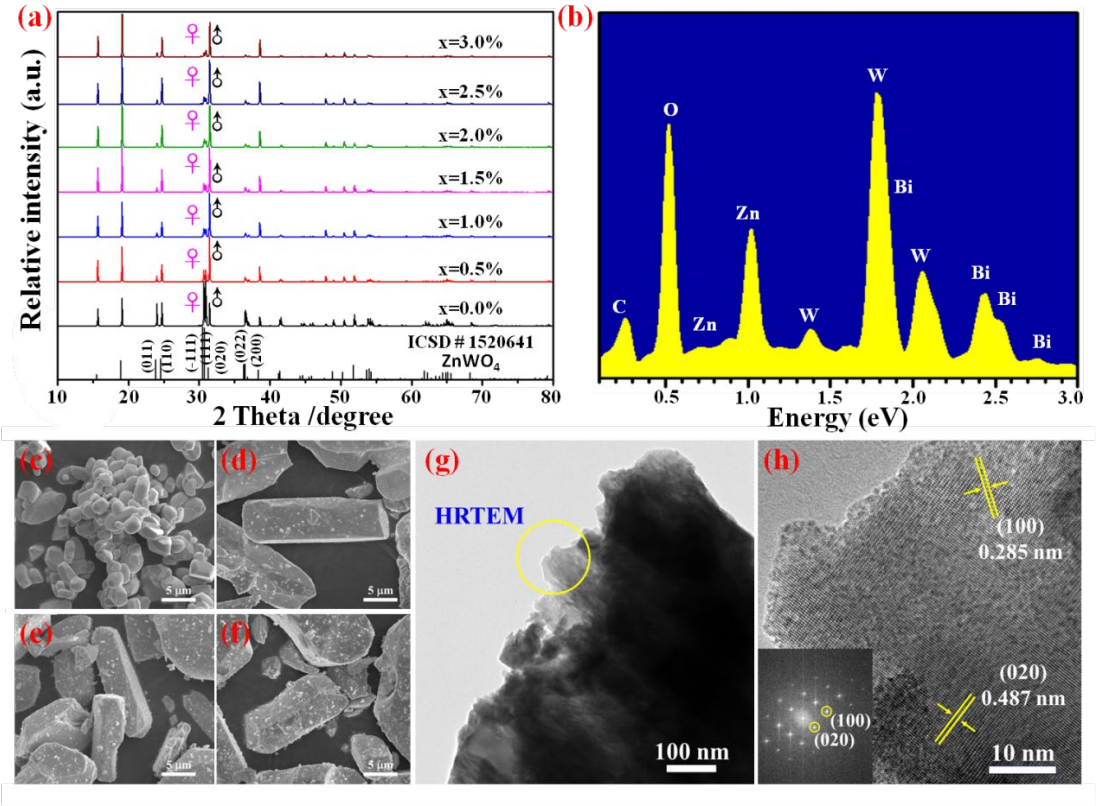
(a)
Relative intensity (a.u.)
x=3.0%
x=2.5%
x=2.0%
x=1.5%
x=1.0%
x=0.5%
x=0.0%
ICSD # 1520641
ZnWO4
(011)
(110)
(-111)
(111)
(020)
(022)
(200)
10 20 30 40 50 60 70 80
2 Theta /degree
(b)
O
W
Zn
Bi
C
Zn
W
W
Bi
Bi
Bi
0.5 1.0 1.5 2.0 2.5 3.0
Energy (eV)
(c)
(d)
(e)
(f)
5 μm
(g)
HRTEM
100 nm
(h)
(100)
0.285 nm
(020)
0.487 nm
(100)
(020)
10 nm

Figure 2

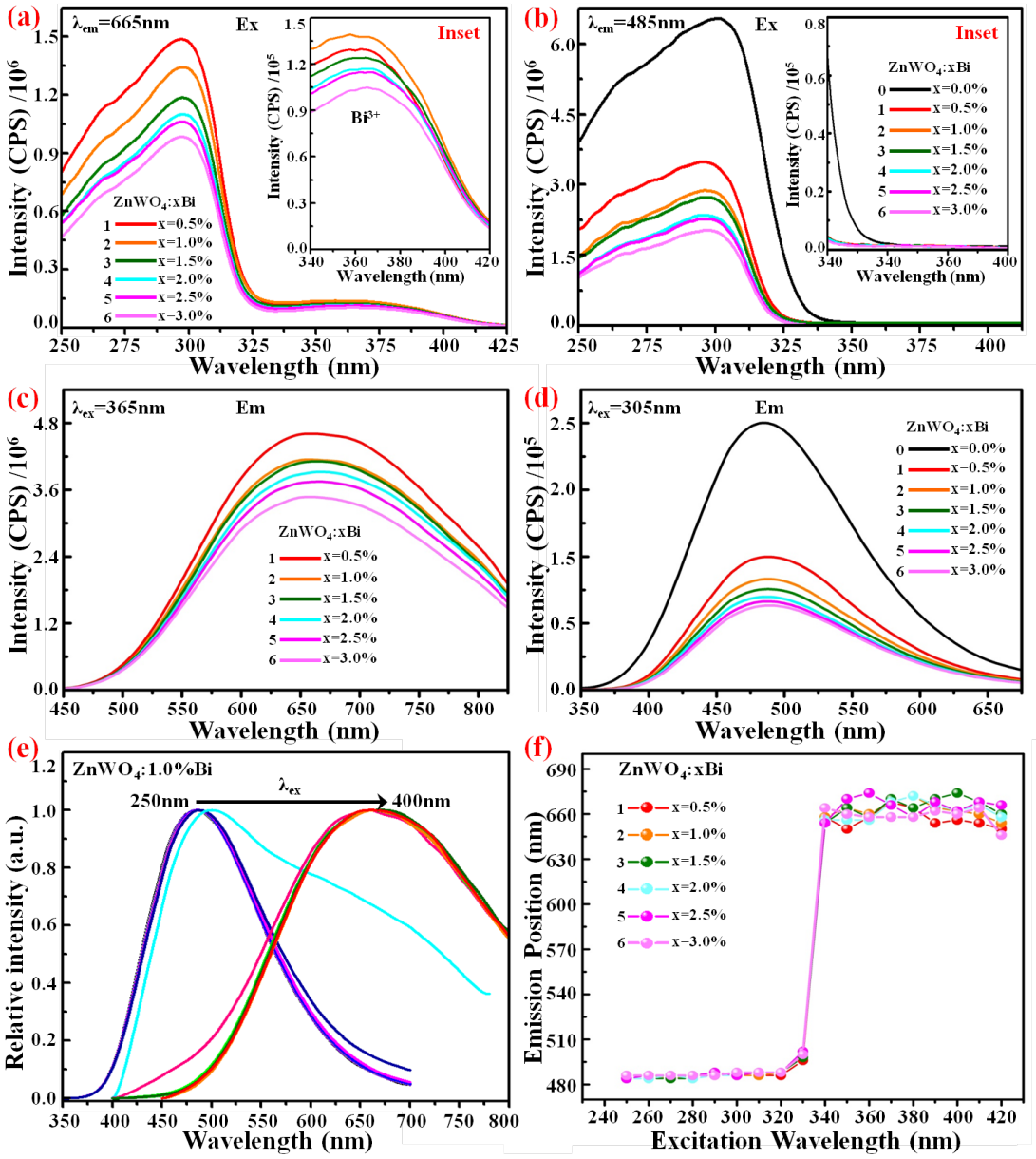
(a)
λem=665nm
Ex
Inset
Bi3+
Intensity (CPS) /10^6
Intensity (CPS) /10^5
Wavelength (nm)
ZnWO4:xBi
1 x=0.5%
2 x=1.0%
3 x=1.5%
4 x=2.0%
5 x=2.5%
6 x=3.0%
(b)
λem=485nm
Ex
Inset
Intensity (CPS) /10^6
Intensity (CPS) /10^5
Wavelength (nm)
ZnWO4:xBi
0 x=0.0%
1 x=0.5%
2 x=1.0%
3 x=1.5%
4 x=2.0%
5 x=2.5%
6 x=3.0%
(c)
λex=365nm
Em
Intensity (CPS) /10^6
Wavelength (nm)
ZnWO4:xBi
1 x=0.5%
2 x=1.0%
3 x=1.5%
4 x=2.0%
5 x=2.5%
6 x=3.0%
(d)
λex=305nm
Em
Intensity (CPS) /10^5
Wavelength (nm)
ZnWO4:xBi
0 x=0.0%
1 x=0.5%
2 x=1.0%
3 x=1.5%
4 x=2.0%
5 x=2.5%
6 x=3.0%
(e)
ZnWO4:1.0%Bi
λex
250nm
400nm
Relative intensity (a.u.)
Wavelength (nm)
(f)
ZnWO4:xBi
1 x=0.5%
2 x=1.0%
3 x=1.5%
4 x=2.0%
5 x=2.5%
6 x=3.0%
Emission Position (nm)
Excitation Wavelength (nm)

Figure 3

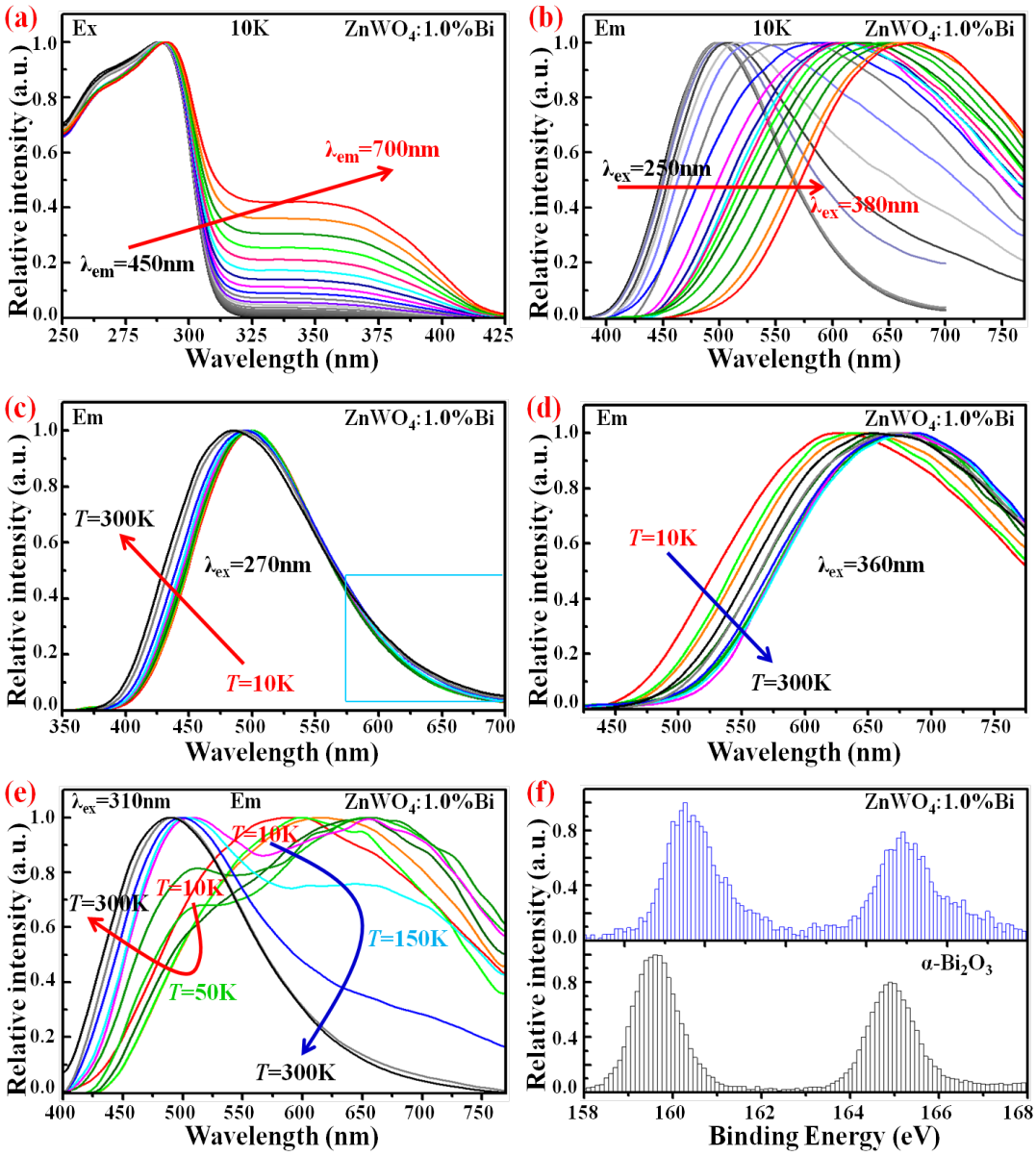
(a)
Ex
10K
ZnWO4:1.0%Bi
λem=700nm
λem=450nm
Relative intensity (a.u.)
Wavelength (nm)
(b)
Em
10K
ZnWO4:1.0%Bi
λex=250nm
λex=380nm
Relative intensity (a.u.)
Wavelength (nm)
(c)
Em
ZnWO4:1.0%Bi
T=300K
λex=270nm
T=10K
Relative intensity (a.u.)
Wavelength (nm)
(d)
Em
ZnWO4:1.0%Bi
T=10K
λex=360nm
T=300K
Relative intensity (a.u.)
Wavelength (nm)
(e)
λex=310nm
Em
ZnWO4:1.0%Bi
T=10K
T=10K
T=300K
T=150K
T=50K
T=300K
Relative intensity (a.u.)
Wavelength (nm)
(f)
ZnWO4:1.0%Bi
α-Bi2O3
Relative intensity (a.u.)
Binding Energy (eV)

Figure 4

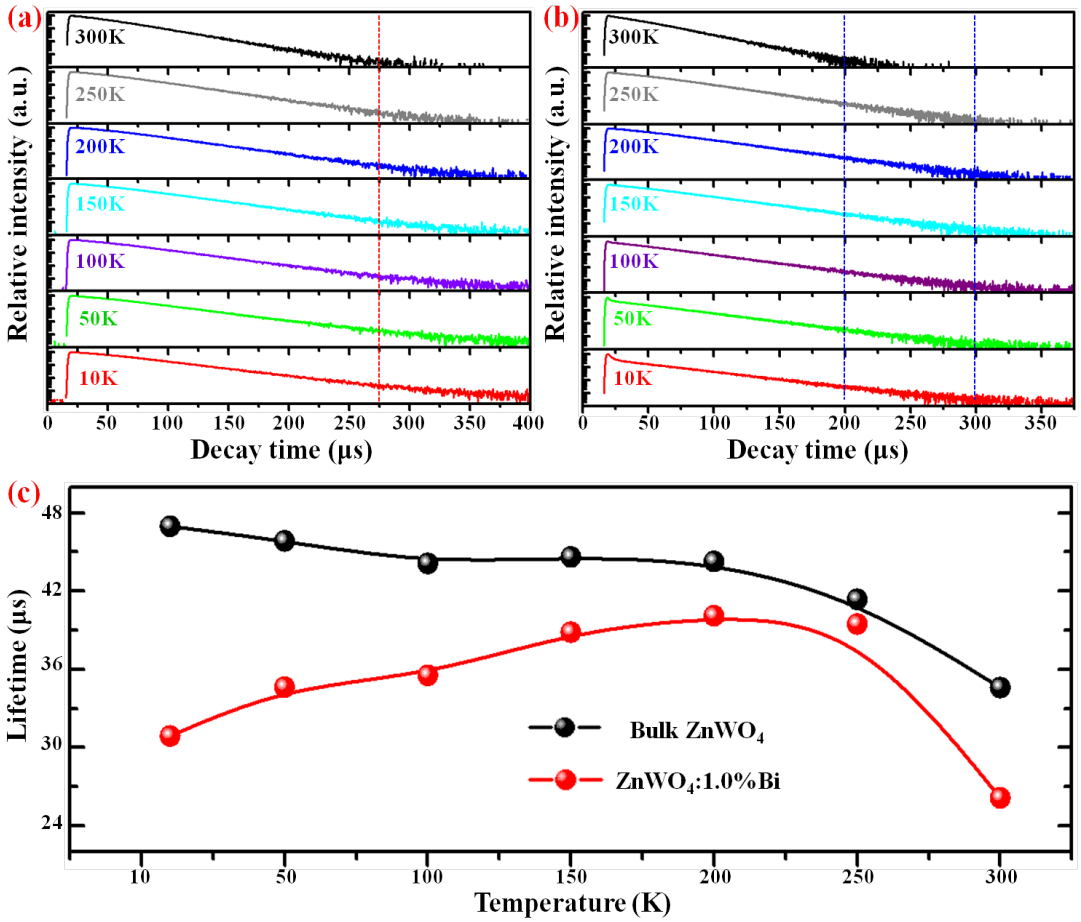
(a)
300K
250K
200K
150K
100K
50K
10K
Relative intensity (a.u.)
0 50 100 150 200 250 300 350 400
Decay time (μs)
(b)
300K
250K
200K
150K
100K
50K
10K
Relative intensity (a.u.)
0 50 100 150 200 250 300 350
Decay time (μs)
(c)
Lifetime (μs)
48
42
36
30
24
Bulk ZnWO4
ZnWO4:1.0%Bi
10 50 100 150 200 250 300
Temperature (K)

Figure 5

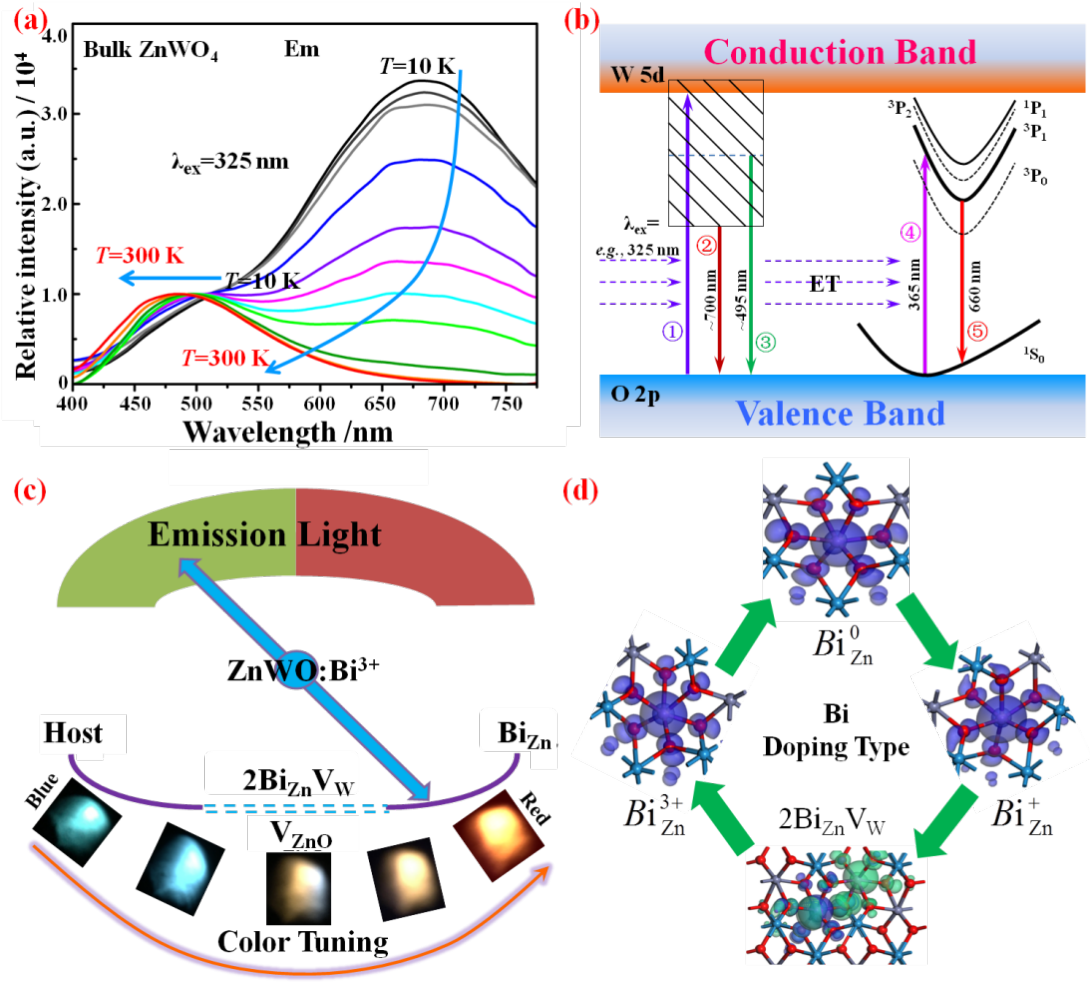
(a)
Bulk ZnWO4
Em
T=10 K
λex=325 nm
T=300 K
T=10 K
T=300 K
Relative intensity (a.u.) / 10⁴
Wavelength /nm
(b)
Conduction Band
W 5d
O 2p
Valence Band
λex=
e.g., 325 nm
~700 nm
~495 nm
ET
365 nm
660 nm
(c)
Emission Light
ZnWO:Bi3+
Host
BiZn
2BiZnVW
VZnO
Blue
Red
Color Tuning
(d)
Bi
Doping Type
2BiZnVW

Figure 6

REFERENCES

(1) Nakamura, S. Blue-Green Light-Emitting Diodes and Violet Laser Diodes. *MRS bulletin* **1997**, *22*, 29-35.

(2) Schubert, E. F.; Kim, J. K. Solid-State Light Sources Getting Smart. *Science* **2005**, *308*, 1274-1278.

(3) Pimputkar, S.; Speck, J. S.; DenBaars, S. P.; Nakamura, S. Prospects for LED Lighting. *Nat. Photon.* **2009**, *3*, 180-182.

(4) Pust, P.; Schmidt, P. J.; Schnick, W. A Revolution in Lighting. *Nat. Mater.* **2015**, *14*, 454-458.

(5) Lin, C. C.; Liu, R. S. Advances in Phosphors for Light-Emitting Diodes. *J. Phys. Chem. Lett.* **2011**, *2*, 1268-1277.

(6) Hirosaki, N.; Takeda, T.; Funahashi, S.; Xie, R. J. Discovery of New Nitridosilicate Phosphors for Solid State Lighting by the Single-Particle-Diagnosis Approach. *Chem. Mater.* **2014**, *26*, 4280-4288.

(7) Xia, Z. G.; Ma, C. G.; Molokeev, M. S.; Liu, Q. L.; Rickert, K.; Poeppelmeier, K. R. Chemical Unit Cosubstitution and Tuning of Photoluminescence in the $Ca_2(Al_{1-x}Mg_x)(Al_{1-x}Si_{1+x})O_7:Eu^{2+}$ Phosphor. *J. Am. Chem. Soc.* **2015**, *137*, 12494-12497.

(8) Wang, B.; Lin, H.; Huang, F.; Xu, J.; Chen, H.; Lin, Z. B.; Wang, Y. S. Non-Rare-Earth $BaMgAl_{10-2x}O_{17}:xMn^{4+},xMg^{2+}$: A Narrow-Band Red Phosphor for Use as a High-Power Warm W-LED. *Chem. Mater.* **2016**, *28*, 3515-3524.

(9) Ratnam, B. V.; Jayasimhadri, M.; Bhaskar Kumar, G.; Jang, K.; Kim, S. S.; Lee, Y. I.; Lim, J. M.; Shin, D. S.; Song, T. K. Synthesis and Luminescent Features of $NaCaPO_4:Tb^{3+}$ Green Phosphor for Near UV-Based LEDs. *J. Alloys Compd.* **2013**, *564*, 100-104.

(10) Liu, Y. F.; Zhang, X.; Hao, Z. D.; Wang, X. J.; Zhang, J. H. Tunable Full-Color-Emitting $Ca_3Sc_2Si_3O_{12}:Ce^{3+}$, Mn^{2+} Phosphor via Charge Compensation and Energy Transfer. *Chem. Commun.*

2011, *47*, 10677-10679.

(11) Takeda, T.; Hirosaki, N.; Funahshi, S.; Xie, R. J. Narrow-Band Green-Emitting Phosphor $Ba_2LiSi_7AlN_{12}:Eu^{2+}$ with High Thermal Stability Discovered by a Single Particle Diagnosis Approach. *Chem. Mater.* **2015**, *27*, 5892-5898.

(12) Hermus, M.; Phan, P.-C.; Brgoch, J. Ab Initio Structure Determination and Photoluminescent Properties of an Efficient, Thermally Stable Blue Phosphor, $Ba_2Y_5B_5O_{17}:Ce^{3+}$. *Chem. Mater.* **2016**, *28*, 1121-1127.

(13) Guo, C. F.; Luan, L.; Chen, C. H.; Huang, D. X.; Su, Q. Preparation of $Y_2O_2S:Eu^{3+}$ Phosphors by a Novel Decomposition Method. *Mater. Lett.* **2008**, *62*, 600-602.

(14) Pust, P.; Weiler, V.; Hecht, C.; Tücks, A.; Wochnik, A. S.; Henß, A.-K.; Wiechert, D.; Scheu, C.; Schmidt, P. J.; Schnick, W. Narrow-Band Red-Emitting $Sr[LiAl_3N_4]:Eu^{2+}$ as a Next-Generation LED-Phosphor Material. *Nat. Mater.* **2014**, *13*, 891-896.

(15) Zhang, S.; Liang, H. B.; Liu, C. M. Increased $^1D_2$ Red Emission of Pr^{3+} in $NaGdTiO_4:Pr^{3+}$ Due to Temperature-Assisted Host Sensitization and Its Color Variation. *J. Phys. Chem. C* **2013**, *117*, 2216-2221.

(16) Wang, L. L.; Noh, H. M.; Moon, B. K.; Park, S. H.; Kim, K. H.; Shi, J. S.; Jeong, J. H. Dual-Mode Luminescence with Broad Near UV and Blue Excitation Band from $Sr_2CaMoO_6:Sm^{3+}$ Phosphor for White LEDs. *J. Phys. Chem. C* **2015**, *119*, 15517-15525.

(17) Wang, B.; Lin, H.; Xu, J.; Chen, H.; Wang, Y. S. $CaMg_2Al_{16}O_{27}:Mn^{4+}$-based Red Phosphor: A Potential Color Converter for High-Powered Warm W-LED. *ACS Appl. Mater. Interfaces* **2014**, *6*, 22905-22913.

(18) Li, M. Q.; Zhang, J. L.; Han, J.; Qiu, Z. X.; Zhou, W. L.; Yu, L. P.; Li, Z. Q.; Lian, S. X. Changing

Ce^{3+} Content and Codoping Mn^{2+} Induced Tunable Emission and Energy Transfer in $Ca_{2.5}Sr_{0.5}Al_2O_6:Ce^{3+},Mn^{2+}$. *Inorg. Chem.* **2017**, *56*, 241-251.

(19) Park, W. B.; Kim, H.; Park, H.; Yoon, C.; Sohn, K.-S. The Composite Structure and Two-Peak Emission Behavior of a $Ca_{1.5}Ba_{0.5}Si_5O_3N_6:Eu^{2+}$ Phosphor. *Inorg. Chem.* **2016**, *55*, 2534-2543.

(20) Geng, D. L.; Li, G. G.; Shang, M. M.; Yang, D. M.; Zhang, Y.; Cheng, Z. Y.; Lin, J. Color Tuning via Energy Transfer in $Sr_3In(PO_4)_3:Ce^{3+}/Tb^{3+}/Mn^{2+}$ Phosphors. *J. Mater. Chem.* **2012**, *22*, 14262-14271.

(21) Miao, S. H.; Xia, Z. G.; Zhang, J.; Liu, Q. L. Increased Eu^{2+} Content and Codoping Mn^{2+} Induced Tunable Full-Color Emitting Phosphor $Ba_{1.55}Ca_{0.45}SiO_4:Eu^{2+},Mn^{2+}$. *Inorg. Chem.* **2014**, *53*, 10386-10393.

(22) Jia, G.; Liu, K.; Zheng, Y. H.; Song, Y. H.; You, H. P. Facile Synthesis and Luminescence Properties of Highly Uniform $MF/YVO_4:Ln^{3+}$ (Ln = Eu, Dy, and Sm) Composite Microspheres. *Cryst. Growth Des.* **2009**, *9*, 3702-3706.

(23) Chen, L.; Chen, K. J.; Hu, S. F.; Liu, R. S. Combinatorial Chemistry Approach to Searching Phosphors for White Light-Emitting Diodes in (Gd-Y-Bi-Eu)VO_4 Quaternary System. *J. Mater. Chem.* **2011**, *21*, 3677-3685.

(24) Lü, W.; Hao, Z. D.; Zhang, X.; Luo, Y. S.; Wang, X. J.; Zhang, J. H. Tunable Full-Color Emitting $BaMg_2Al_6Si_9O_{30}:Eu^{2+}$, Tb^{3+}, Mn^{2+} Phosphors Based on Energy Transfer. *Inorg. Chem.* **2011**, *50*, 7846-7851.

(25) Liu, Y.; Liu, G. X.; Wang, J. X.; Dong, X. T.; Yu, W. S. Single-Component and Warm-White-Emitting Phosphor $NaGd(WO_4)_2:Tm^{3+}$, Dy^{3+}, Eu^{3+}: Synthesis, Luminescence, Energy Transfer, and Tunable Color. *Inorg. Chem.* **2014**, *53*, 11457-11466.

(26) Geng, D. L.; Shang, M. M.; Zhang, Y.; Lian, H. Z.; Lin, J. Color-Tunable and White Luminescence Properties via Energy Transfer in Single-Phase $KNaCa_2(PO_4)_2$:A (A = Ce^{3+}, Eu^{2+}, Tb^{3+}, Mn^{2+}, Sm^{3+}) Phosphors. *Inorg. Chem.* **2013**, *52*, 13708-13718.

(27) Blasse, G.; Bril, A. Investigations on Bi^{3+}-Activated Phosphors. *J. Chem. Phys.* **1968**, *48*, 217-222.

(28) Kang, F. W.; Peng, M. Y.; Yang, X. B.; Dong, G. P.; Nie, G. C.; Liang, W. J.; Xu, S. H.; Qiu, J. R. Broadly Tuning Bi^{3+} Emission via Crystal Field Modulation in Solid Solution Compounds (Y,Lu,Sc)VO_4:Bi for Ultraviolet Converted White LEDs. *J. Mater. Chem. C* **2014**, *2*, 6068-6076.

(29) Kang, F. W.; Zhang, H. S.; Wondraczek, L.; Yang, X. B.; Zhang, Y.; Lei, D. Y.; Peng, M. Y. Band-Gap Modulation in Single Bi^{3+}-Doped Yttrium-Scandium-Niobium Vanadates for Color Tuning over the Whole Visible Spectrum. *Chem. Mater.* **2016**, *28*, 2692-2703.

(30) Vehse, W. E.; Sherrill, F. A.; Riley, C. R. Lattice Constants for $KMg_{(1-x)}Mn_xF_3$ Crystals. *J. Appl. Phys.* **1972**, *43*, 1320-1321.

(31) Dai, P. P.; Zhang, X. T.; Bian, L. L.; Lu, S.; Liu, Y. C.; Wang, X. J. Color Tuning of (K_{1-x},Na_x)$SrPO_4$:0.005Eu^{2+}, yTb^{3+} Blue-Emitting Phosphors via Crystal Field Modulation and Energy Transfer. *J. Mater. Chem. C* **2013**, *1*, 4570-4576.

(32) Wu, Q. S.; Yang, Z. G.; Zhao, Z. Y.; Que, M. D.; Wang, X. C.; Wang, Y. H. Synthesis, Crystal Structure and Luminescence Properties of a $Y_4Si_2O_7N_2$:Ce^{3+} Phosphor for Near-UV White LEDs. *J. Mater. Chem. C* **2014**, *2*, 4967-4973.

(33) Sato, Y.; Kato, H.; Kobayashi, M.; Masaki, T.; Yoon, D.-H.; Kakihana, M. Tailoring of Deep-Red Luminescence in Ca_2SiO_4:Eu^{2+}. *Angew. Chem. Int. Ed.* **2014**, *53*, 7756-7759.

(34) Lian, S. X.; Rong, C. Y.; Yin, D. L.; Liu, S. B. Enhancing Solar Energy Conversion Efficiency: A Tunable Dual-Excitation Dual-Emission Phosphors and Time-Dependent Density Functional Theory

Study. *J. Phys. Chem. C* **2009**, *113*, 6298-6302.

(35) Park, W. B.; Singh, S. P.; Yoon, C.; Sohn, K.-S. Eu^{2+} Luminescence from 5 Different Crystallographic Sites in a Novel Red Phosphor, $Ca_{15}Si_{20}O_{10}N_{30}:Eu^{2+}$. *J. Mater. Chem.* **2012**, *22*, 14068-14075.

(36) Kang, F. W.; Yang, X. B.; Peng, M. Y.; Wondraczek, L.; Ma, Z. J.; Zhang, Q. Y.; Qiu, J. R. Red Photoluminescence from Bi^{3+} and the Influence of the Oxygen-Vacancy Perturbation in $ScVO_4$: A Combined Experimental and Theoretical Study. *J. Phys. Chem. C* **2014**, *118*, 7515-7522.

(37) Kraus, H.; Mikhailik, V. B.; Vasylechko, L.; Day, D.; Hutton, K. B.; Telfer, J.; Prots, Y. Effect of Ca Doping on the Structure and Scintillation Properties of $ZnWO_4$. *phys. status solidi (a)* **2007**, *204*, 730-736.

(38) Lin, J.; Lin, J.; Zhu, Y. F. Controlled Synthesis of the $ZnWO_4$ Nanostructure and Effects on the Photocatalytic Performance. *Inorg. Chem.* **2007**, *46*, 8372-8378.

(39) Shim, H.-W.; Cho, I.-S.; Hong, K. S.; Lim, A.-H.; Kim, D.-W. Wolframite-Type $ZnWO_4$ Nanorods as New Anodes for Li-Ion Batteries. *J. Phys. Chem. C* **2011**, *115*, 16228-16233.

(40) Clark Stewart, J.; Segall Matthew, D.; Pickard Chris, J.; Hasnip Phil, J.; Probert Matt, I. J.; Refson, K.; Payne Mike, C. First Principles Methods Using CASTEP. In *Zeitschrift für Kristallographie - Crystalline Materials*, 2005; Vol. 220, p 567.

(41) Pickard, C. J.; Winkler, B.; Chen, R. K.; Payne, M. C.; Lee, M. H.; Lin, J. S.; White, J. A.; Milman, V.; Vanderbilt, D. Structural Properties of Lanthanide and Actinide Compounds within the Plane Wave Pseudopotential Approach. *Phys. Rev. Lett.* **2000**, *85*, 5122-5125.

(42) Huang, B. L. 4*f* Fine-Structure Levels as the Dominant Error in the Electronic Structures of Binary Lanthanide Oxides. *J. Comput. Chem.* **2016**, *37*, 825-835.

(43) Huang, B. L. Intrinsic Deep Hole Trap Levels in Cu_2O with Self-Consistent Repulsive Coulomb Energy. *Solid State Commun.* **2016**, *230*, 49-53.

(44) Huang, B. L. Strong Compensation Hinders the p-Type Doping of ZnO: A Glance over Surface Defect Levels. *Solid State Commun.* **2016**, *237*, 34-37.

(45) Huang, B. L. The Screened Pseudo-Charge Repulsive Potential in Perturbed Orbitals for Band Calculations by DFT+U. *Phys. Chem. Chem. Phys.* **2017**, *19*, 8008-8025.

(46) Vladimir, I. A.; Aryasetiawan, F.; Lichtenstein, A. I. First-Principles Calculations of the Electronic Structure and Spectra of Strongly Correlated Systems: The LDA + U Method. *J. Phys.: Condens. Matter* **1997**, *9*, 767.

(47) Marzari, N.; Vanderbilt, D.; Payne, M. C. Ensemble Density-Functional Theory for Ab Initio Molecular Dynamics of Metals and Finite-Temperature Insulators. *Phys. Rev. Lett.* **1997**, *79*, 1337-1340.

(48) Probert, M. I. J.; Payne, M. C. Improving the Convergence of Defect Calculations in Supercells: An Ab Initio Study of the Neutral Silicon Vacancy. *Phys. Rev. B* **2003**, *67*, 075204.

(49) Nan, H. Y.; Wang, Z. L.; Wang, W. H.; Liang, Z.; Lu, Y.; Chen, Q.; He, D. W.; Tan, P. H.; Miao, F.; Wang, X. R.; Wang, J. L.; Ni, Z. H. Strong Photoluminescence Enhancement of MoS_2 through Defect Engineering and Oxygen Bonding. *ACS Nano* **2014**, *8*, 5738-5745.

(50) Kang, F. W.; Peng, M. Y.; Zhang, Q. Y.; Qiu, J. R. Abnormal Anti-Quenching and Controllable Multi-Transitions of Bi^{3+} Luminescence by Temperature in a Yellow-Emitting $LuVO_4$:Bi^{3+} Phosphor for UV-Converted White LEDs. *Chem. -Eur. J.* **2014**, *20*, 11522-11530.

(51) Huang, B. L. Energy Harvesting and Conversion Mechanisms for Intrinsic Upconverted Mechano-Persistent Luminescence in CaZnOS. *Phys. Chem. Chem. Phys.* **2016**, *18*, 25946-25974.

(52) Cao, B. Q.; Cai, W. P.; Zeng, H. B. Temperature-Dependent Shifts of Three Emission Bands for ZnO Nanoneedle Arrays. *Appl. Phys. Lett.* **2006**, *88*, 161101.

(53) Kang, F. W.; Peng, M. Y.; Xu, S. H.; Ma, Z. J.; Dong, G. P.; Qiu, J. R. Broadly Tunable Emission from $CaMoO_4$:Bi Phosphor Based on Locally Modifying the Microenvironment around Bi^{3+} Ions. *Eur. J. Inorg. Chem.* **2014**, *2014*, 1373-1380.

(54) Kang, F. W; Peng, M. Y. A New Study on the Energy Transfer in the Color-Tunable Phosphor $CaWO_4$:Bi. *Dalton Trans.* **2014**, *43*, 277-284.

(55) Srivastava, A. M.; Beers, W. W. On the Impurity Trapped Exciton Luminescence in $La_2Zr_2O_7:Bi^{3+}$. *J. Lumin.* **1999**, *81*, 293-300.

(56) Zhang, S. Y.; Gao, F. M.; Wu, C. X. Chemical Bond Properties of Rare Earth Ions in Crystals. *J. Alloys Compd.* **1998**, *275-277*, 835-837.

Figure Captions

Figure 1 (**a**) Lattice cell of $ZnWO_4$ crystal, based on data from Joint Committee on Powder Diffraction Standards (JCPDS) file No. 15-0774; (**b**) The projected electronic density of states (PDOSs) of bulk $ZnWO_4$ crystal; (**c**) and (**d**) The PDOSs properties for the Bi_W and Bi_{Zn} doping types, respectively, denotations have been labeled beside each curve. Single-particle levels of Bi_{Zn} doping type, defect complex model ($2Bi_{Zn}V_W$) and intrinsic defect V_{ZnO} in $ZnWO_4$ crystal with different charge states (red and black curves denote empty and filled states, respectively).

Figure 2 (**a**) XRD patterns of $ZnWO_4$ crystal without and with Bi^{3+} doping; (**b**) EDX pattern for the selected $ZnWO_4$:1.0%Bi^{3+} sample; (**c-f**) SEM images for $ZnWO_4$:$x$$Bi^{3+}$ (x = 0, 1.0%, 2.0%, and 3.0%) samples; (**g**) TEM image for one selected $ZnWO_4$:1.0%Bi^{3+} particle; and (**h**) HRTEM image of selected area from (**g**) and the FFT pattern (**the lower-left corner of inset**).

Figure 3 Excitation (**a-b**) and emission (**c**, **d**) spectra for $ZnWO_4$ phosphors with and without Bi doping, the excitation and the monitored spectral wavelengths as well as the Bi doping content have been denoted besides the figures; (**e**) Emission spectra for selected $ZnWO_4$:1.0%Bi^{3+} sample with changing the excitation wavelength from 250 nm to 400 nm; (**f**) Variation tendency of emission position for all Bi^{3+} doped $ZnWO_4$ phosphors upon excitation at the 250-420 nm range.

Figure 4 (**a**) Excitation spectra of $ZnWO_4$:1.0%Bi^{3+} sample upon monitoring at the emission wavelength from 450 nm to 700 nm, the measured temperature is 10 K; (**b**) Emission spectra of this sample upon excitation at the wavelength range of 250-380 nm, the temperature is 10 K; (**c**), (**d**) and (**e**) are temperature-dependent emission spectra for this sample upon excitation at 270 nm, 360 nm and 310 nm, respectively; (**f**) XPS spectra for the sample (**purple curve**) and α-Bi_2O_3 reference (**black curve**). The rectangular frame of **Figure 4**(**c**) denotes a new emission band.

Figure 5 Temperature dependent PL decay curves (λ_{ex} = 305 nm, λ_{em} = 485 nm) (**a-b**) for bulk

$ZnWO_4$ (**a**) and $ZnWO_4$:1.0%Bi^{3+} phosphors (**b**), and the corresponding fitted lifetimes (**c**).

Figure 6 (**a**) Emission spectra of bulk $ZnWO_4$ sample, the measured temperature range is 10-300 K; (**b**) Schemes for experimental PL observation, ET denotes the energy transfer process from host to Bi^{3+}; (**c**) Schematic diagram for tunable luminescence in $ZnWO_4$:Bi^{3+} phosphor, the tunable emissions can be illustrated by the below photographs; (**d**) Structural information that derives from PDOSs results of **Figure 1**(**d**), denotations for Zn-substituted Bi^0 (*i.e.*, Bi_{Zn}^0), Zn-substituted Bi^+ (*i.e.*, Bi_{Zn}^+) and Zn-substituted Bi^{3+} (*i.e.*, Bi_{Zn}^{3+}) as well as the $2Bi_{Zn}V_W$ charge compensated complex have been labeled beside each pattern.

Table of Contents Graphic

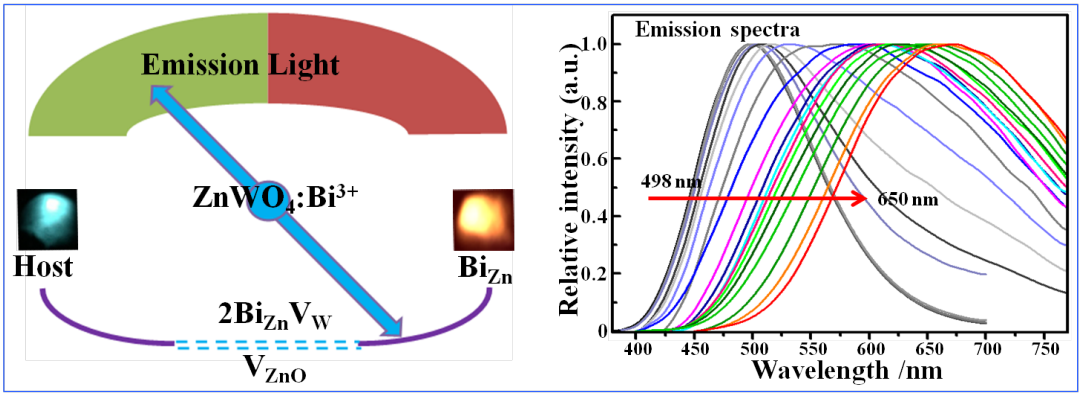

The manageable energy transfer between $ZnWO_4$ host and Bi^{3+}, the V_{ZnO} defect perturbation in the $ZnWO_4$ and the $2Bi_{Zn}V_W$ complex which is produced by substitution of Zn site with Bi^{3+} enable us to achieve the tunable colors and novel Bi^{3+} red luminescence eventually.